

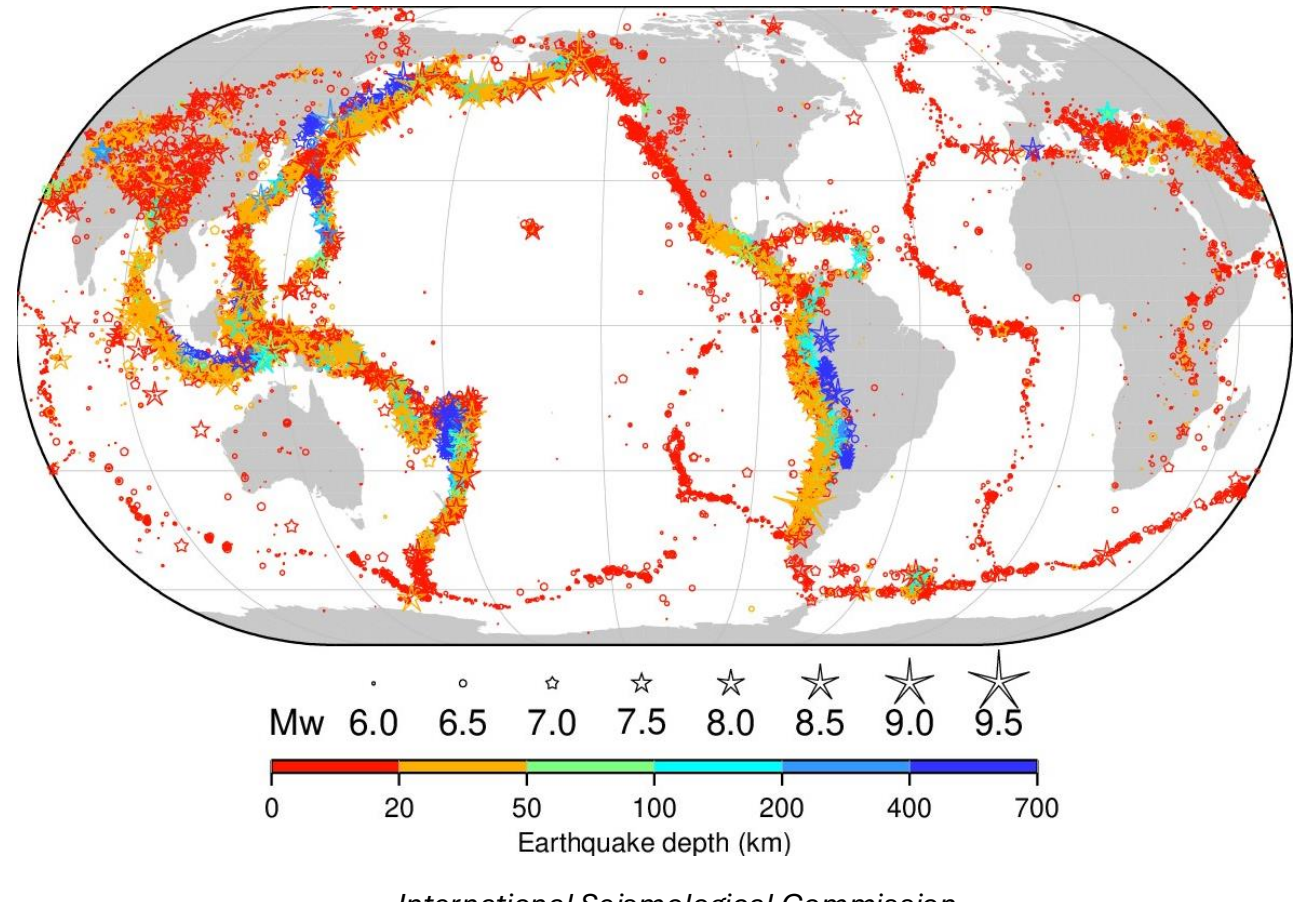
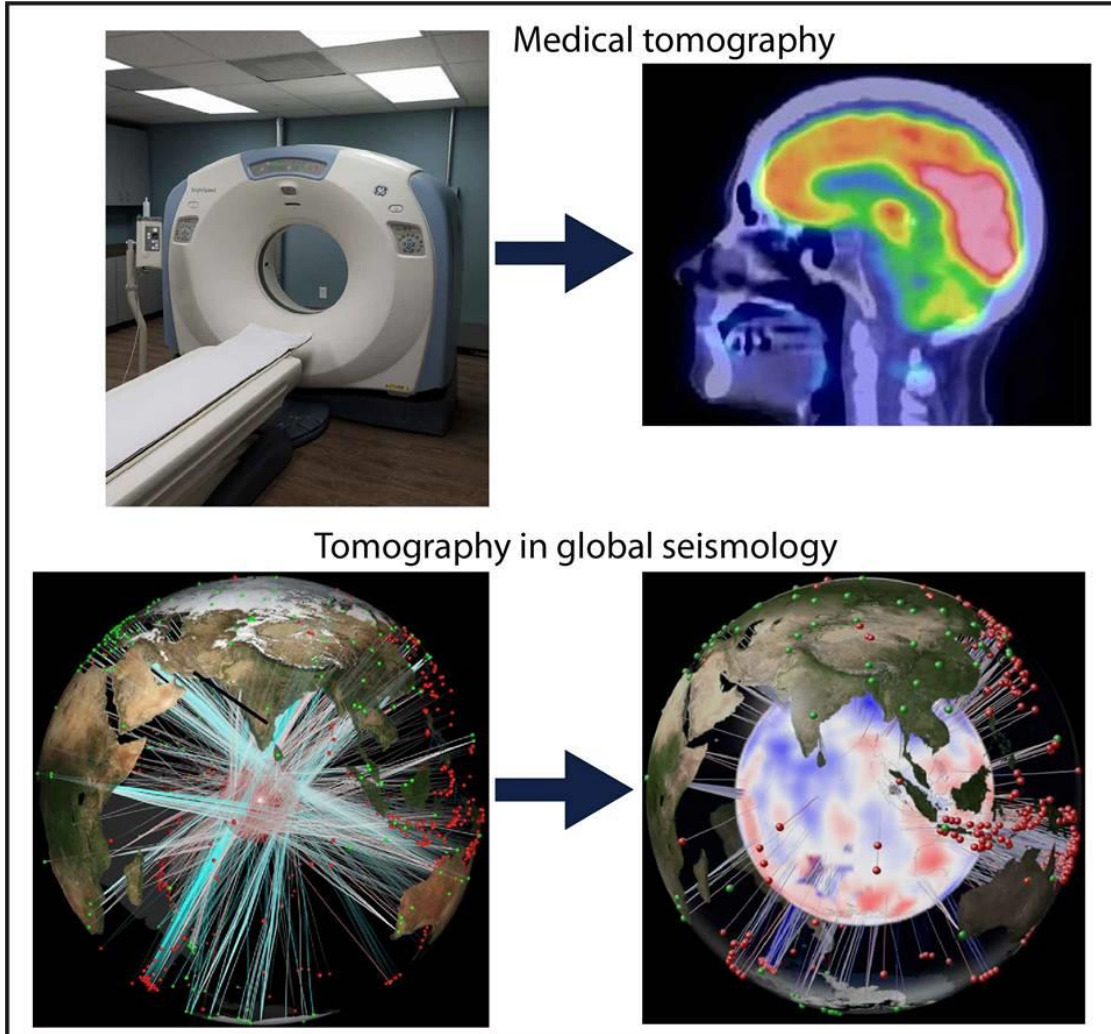
# Lecture 2: Introduction to passive source seismic imaging

OBS training workshop, VUW, April 14-16, 2025

# Content

- Seismic tomography
  - General principles
  - Body-wave travel-time tomography
  - Surface-wave tomography
  - Resolution
- Receiver functions
  - General principles
  - Crustal and mantle structure

# Seismic tomography: General principles



*International Seismological Commission*

Average ~100-120 earthquakes magnitude  $\geq 6.0$  per year

# Body-wave travel-time tomography

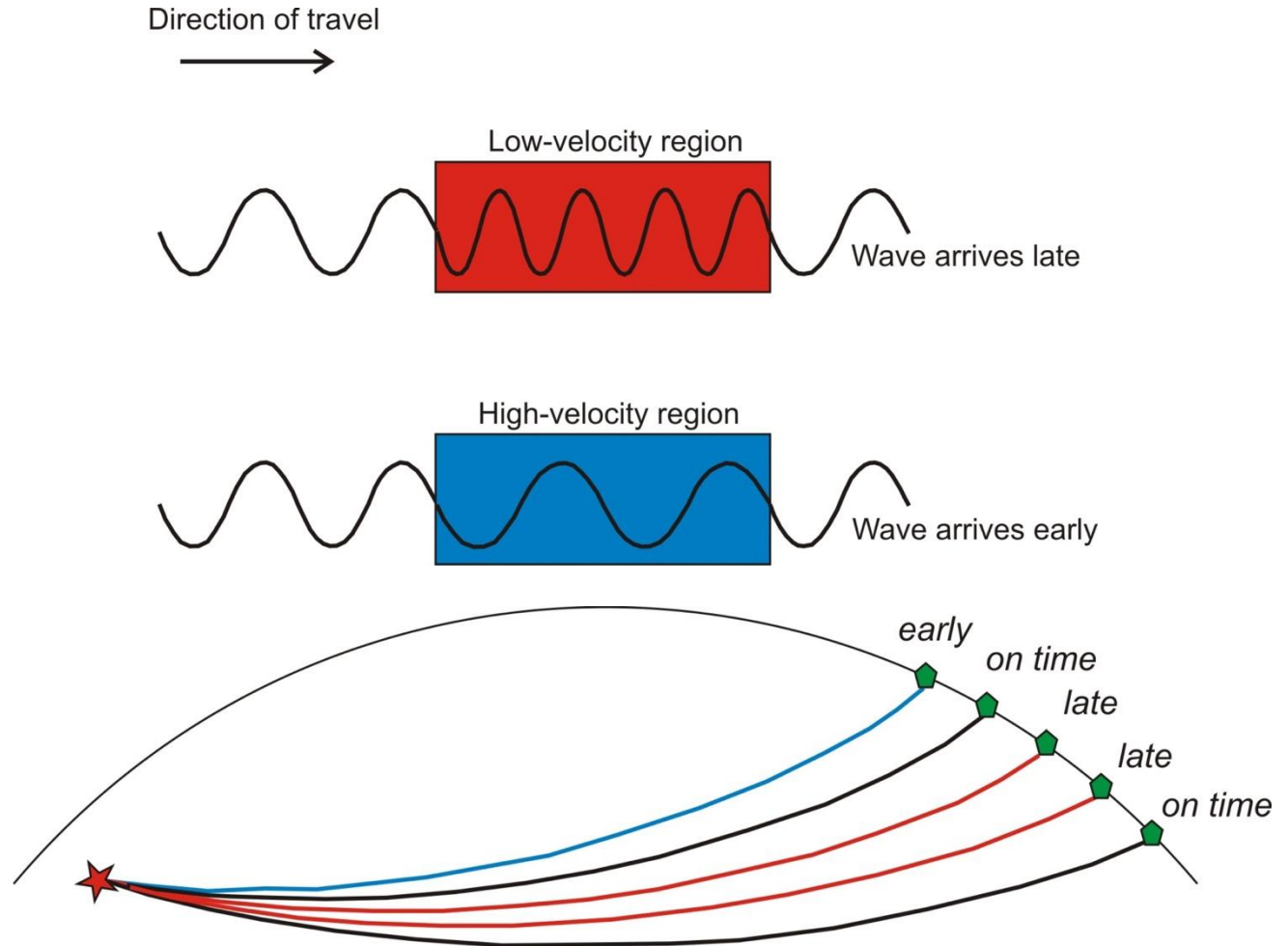
- Measure earthquake travel times and compare to predictions from simple reference models
- Perturbations in travel time → seismic velocity (wavespeed) based structural information
- Basis of measurement: the travel time *residual*

$$\Delta t_A = t_A - t_{r,A} \quad \text{observed - predicted from reference model}$$

- Travel time = integral of wave *slowness* (1/wavespeed) along the source-station raypath

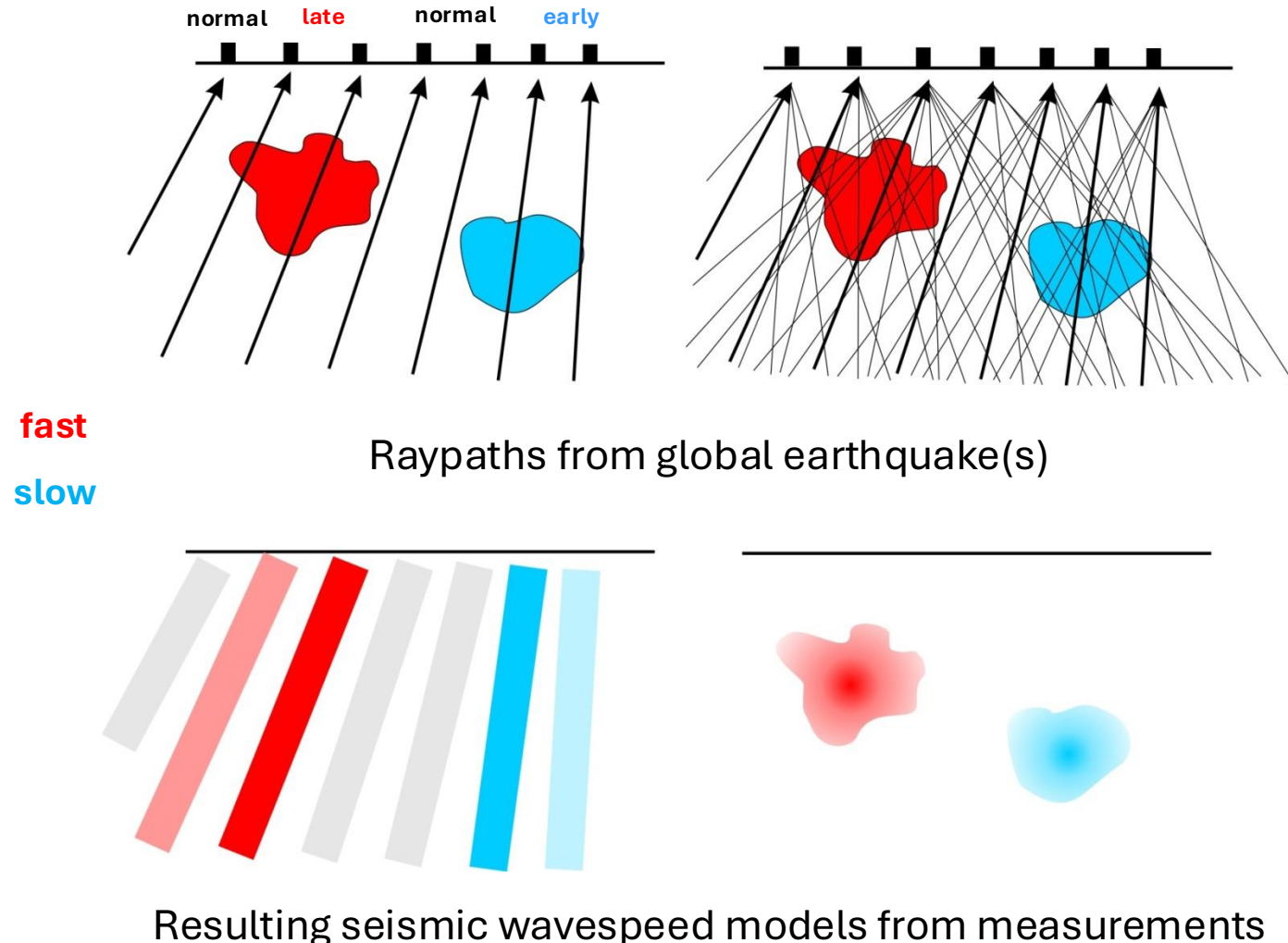
$$\Delta t_A = \int_{rayA} [u(r) - u_r(r)] ds$$

- Challenge: where are the sources of the travel time perturbations?



# Body-wave travel-time tomography

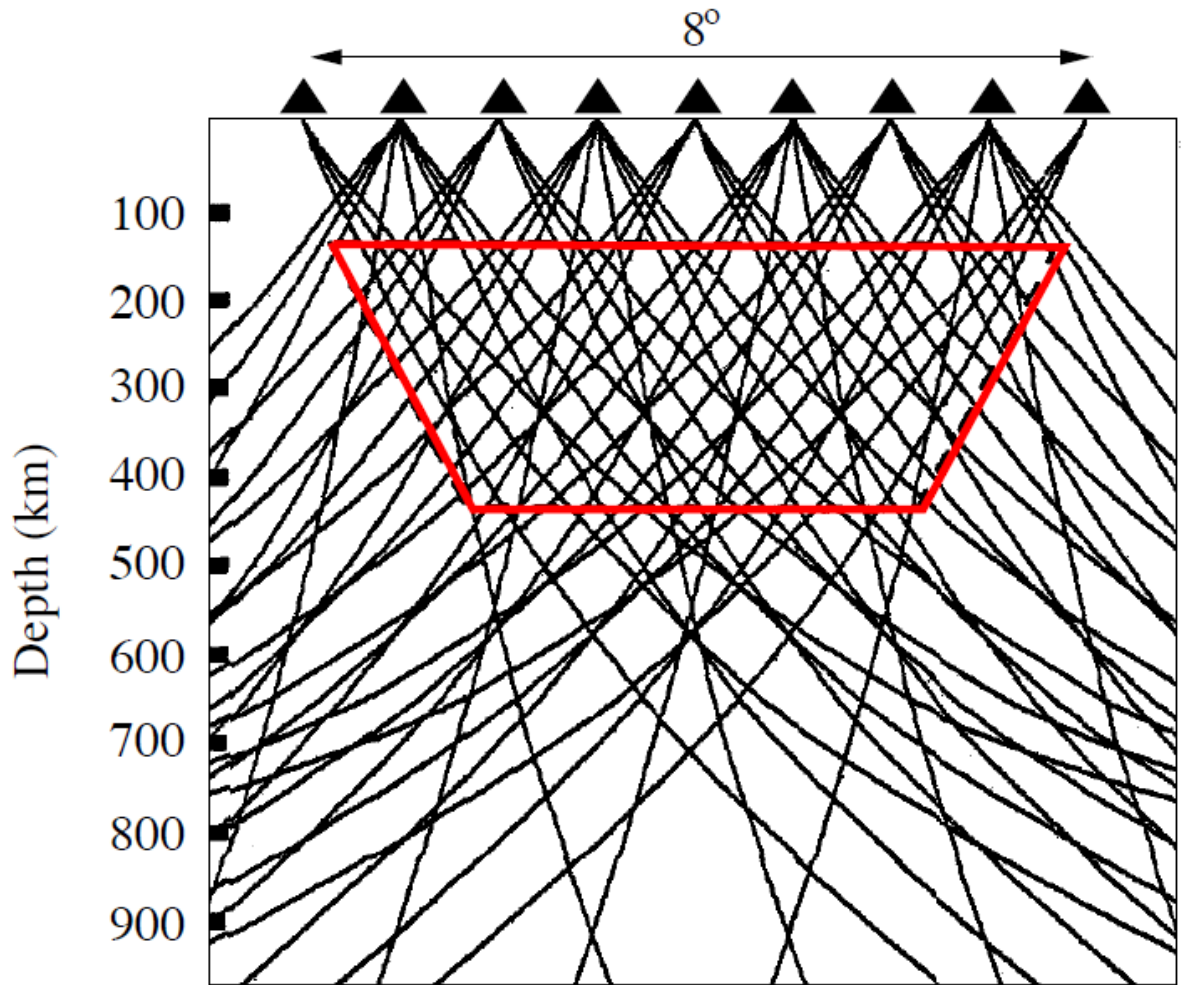
- Anomalies are smeared out along the ray paths (e.g., 1 earthquake, multiple receivers or 1 receiver, multiple earthquakes)
- Requires *crossing* ray paths to localise anomalies beneath the network (i.e., multiple earthquakes, multiple stations)



# Body-wave travel-time tomography

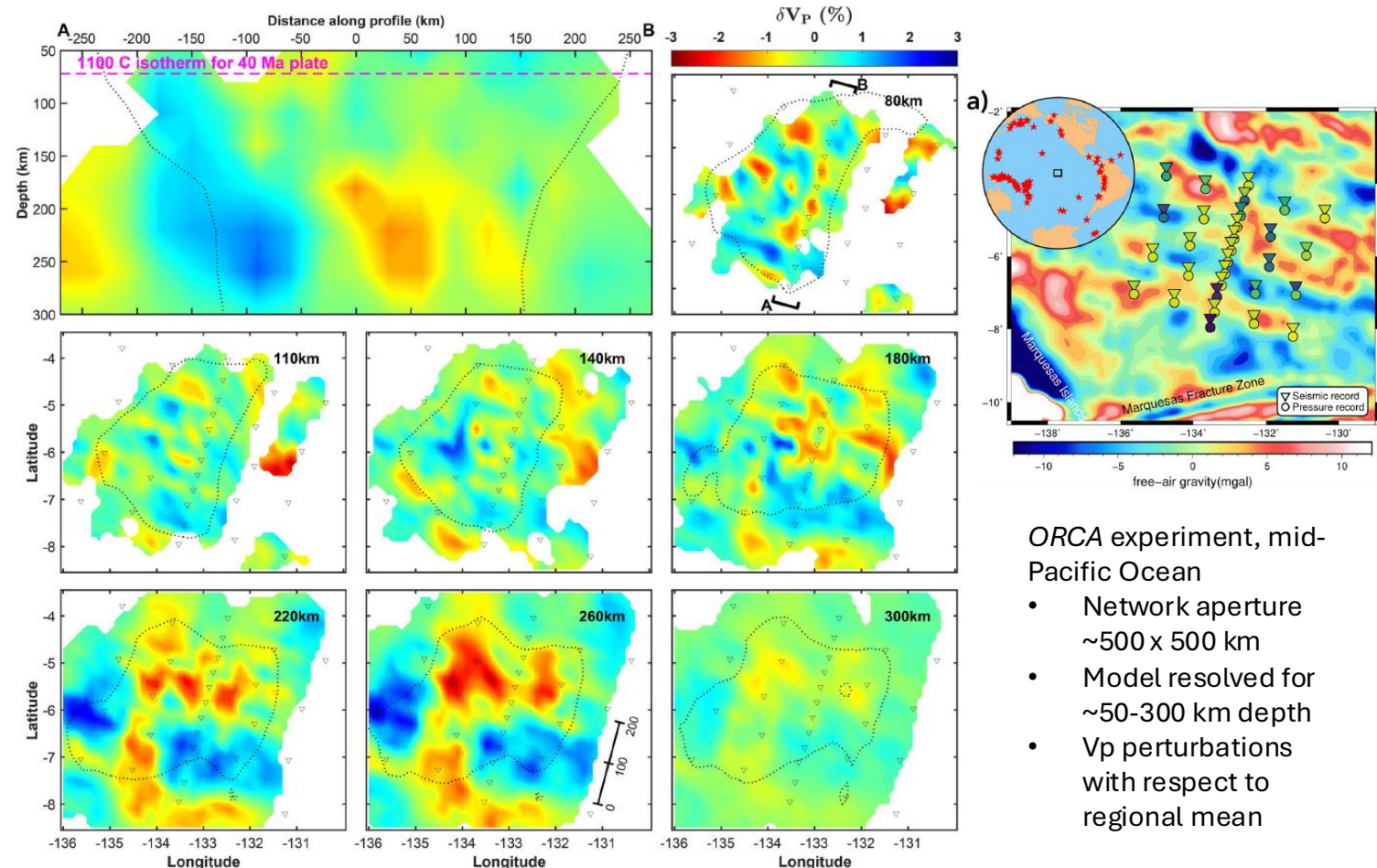
- Depth range of resolvable structure is controlled by (i) station spacing, (ii) total network aperture (width).
- Shallowest resolvable structure  $\approx$  station spacing (due to steep angle of incidence for teleseismic body waves)
- Greatest resolvable depth  $\approx$  network aperture
- Best-resolved depth  $\approx$  between station spacing and  $\frac{1}{2}$  network aperture
- Difficult to resolve crustal depths from teleseismic body wave tomography, even when stations are closely-spaced, due to near-vertical incidence angles at such shallow depths → studies target upper mantle structure.

Station spacing:  $1^\circ$  (111 km); network aperture 888 km



# Body-wave travel-time tomography

- Result: 3D model of perturbations in seismic wavespeed relative to an (unknown) regional mean, expressed in % anomaly.
- Publication figures are presented as horizontal slices (maps) for depths of interest and vertical cross-sections for visualizing 3D structures.
- Regions without crossing ray paths are masked.
- Colour scales vary, but most *mantle* studies use **red** for relatively **slow** structures and **blue** for relatively **fast** structures.
- (NB. Opposite convention to that of many crustal-scale studies, especially those based on active-source data – check the colour bar carefully!)

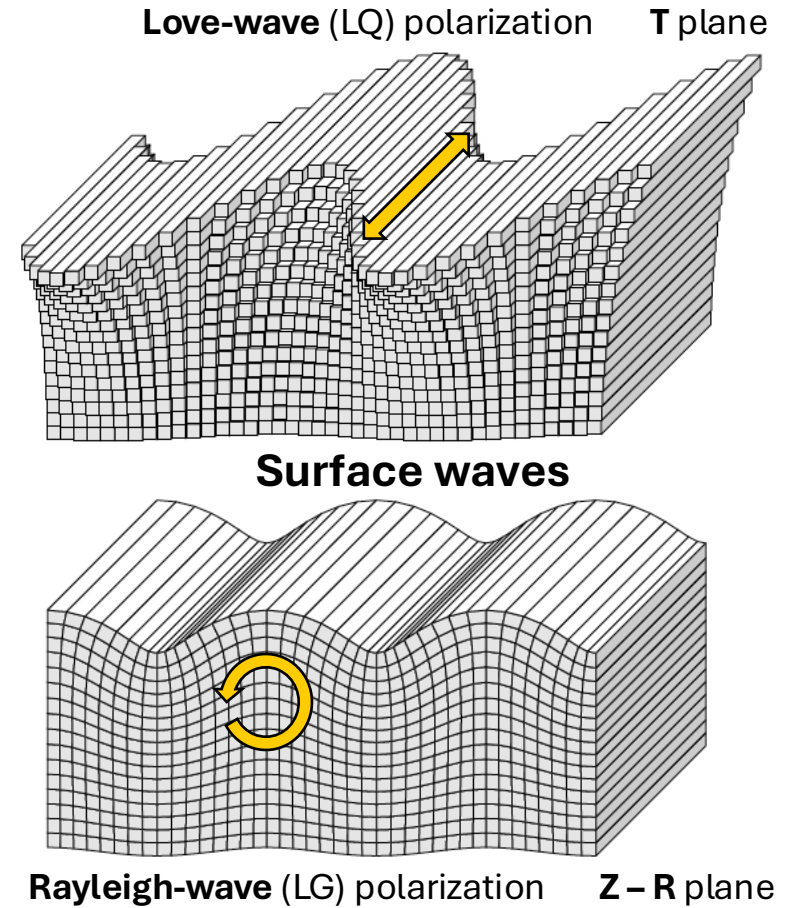


ORCA experiment, mid-Pacific Ocean

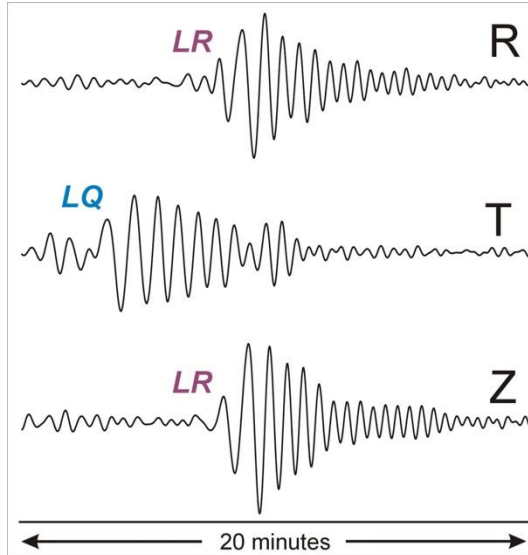
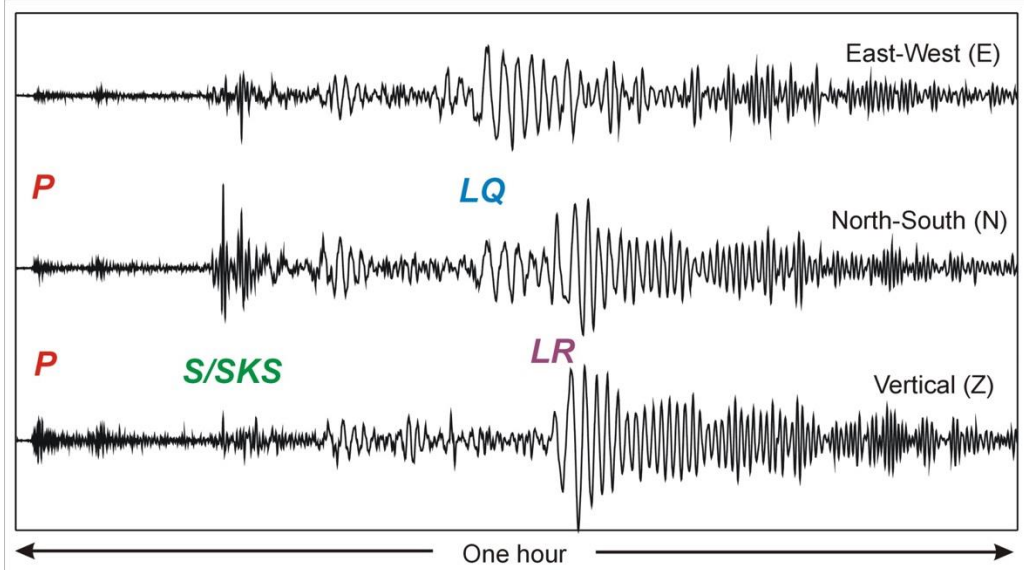
- Network aperture  $\sim 500 \times 500$  km
- Model resolved for  $\sim 50\text{-}300$  km depth
- $V_p$  perturbations with respect to regional mean

# Surface-wave tomography

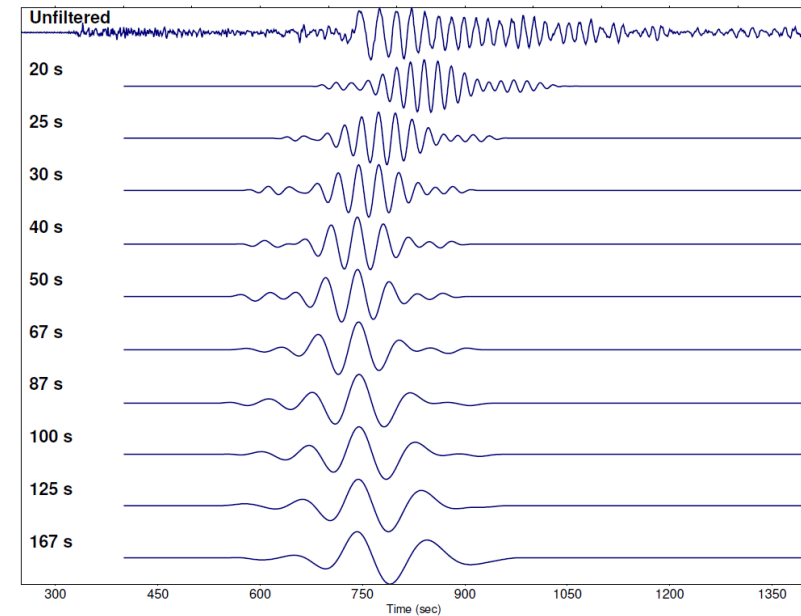
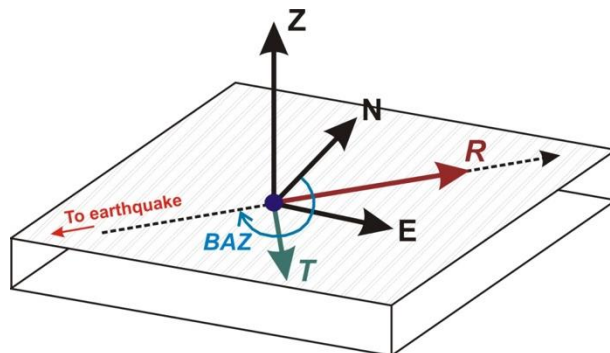
- May use teleseismic or regional earthquakes; azimuthal coverage is important
- Or use *ambient noise* signals, which give rise to properties similar to surface waves (with the right processing)
- Track surface wave propagation
  - From a source (earthquake) to a single station
  - Between a pair of stations
  - Across a closely-spaced array of stations
- Rayleigh (LR) and Love (LQ) waves have sensitivity to shear wavespeed structure in the subsurface



# Surface-wave tomography

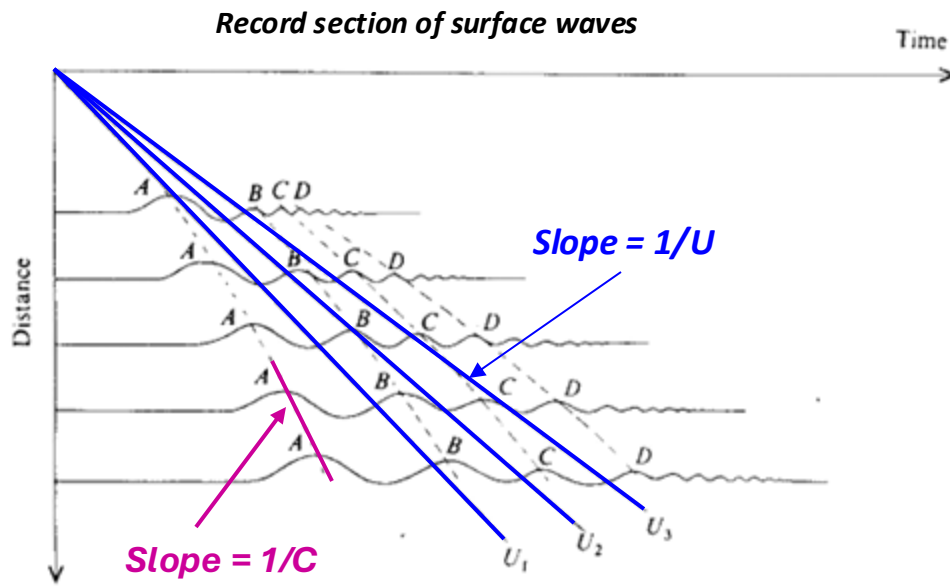


- Rayleigh waves appear on the *vertical* and *radial* component seismograms (→ most widely used, as signal:noise ratio is best on vertical components).
- Love waves appear only on the *tangential (transverse)* component seismogram.
- Propagation speeds: LQ > LR
- Note the change in frequency content with time – waves are *dispersive*; lower frequencies travel faster than higher frequencies

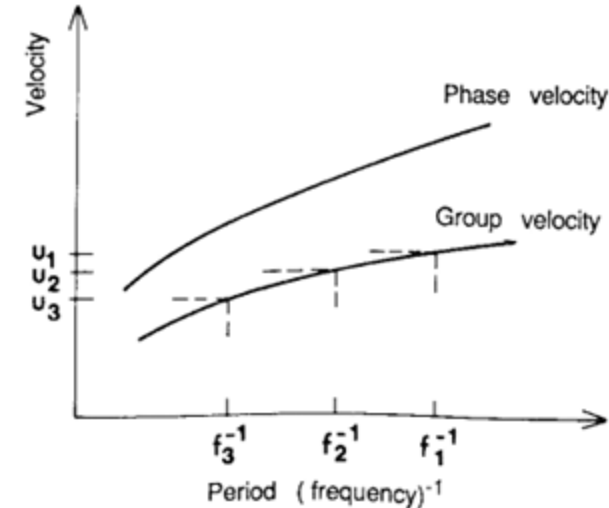


Bagherpur Mojaver et al. (2021)

# Surface-wave tomography



**Dispersion curves** – describe the variation in seismic velocity with frequency:



- **Group velocity ( $U$ )** – velocity associated with a particular frequency in the wave packet
  - Can also be thought of as the velocity at which the entire wave packet (envelope) propagates.
- **Phase velocity ( $C$ )** – velocity of a particular phase, e.g. peak or trough. The frequency of a given phase changes with distance travelled.

$$U(\omega) = d\omega / dk$$

$$C(\omega) = \omega / k$$

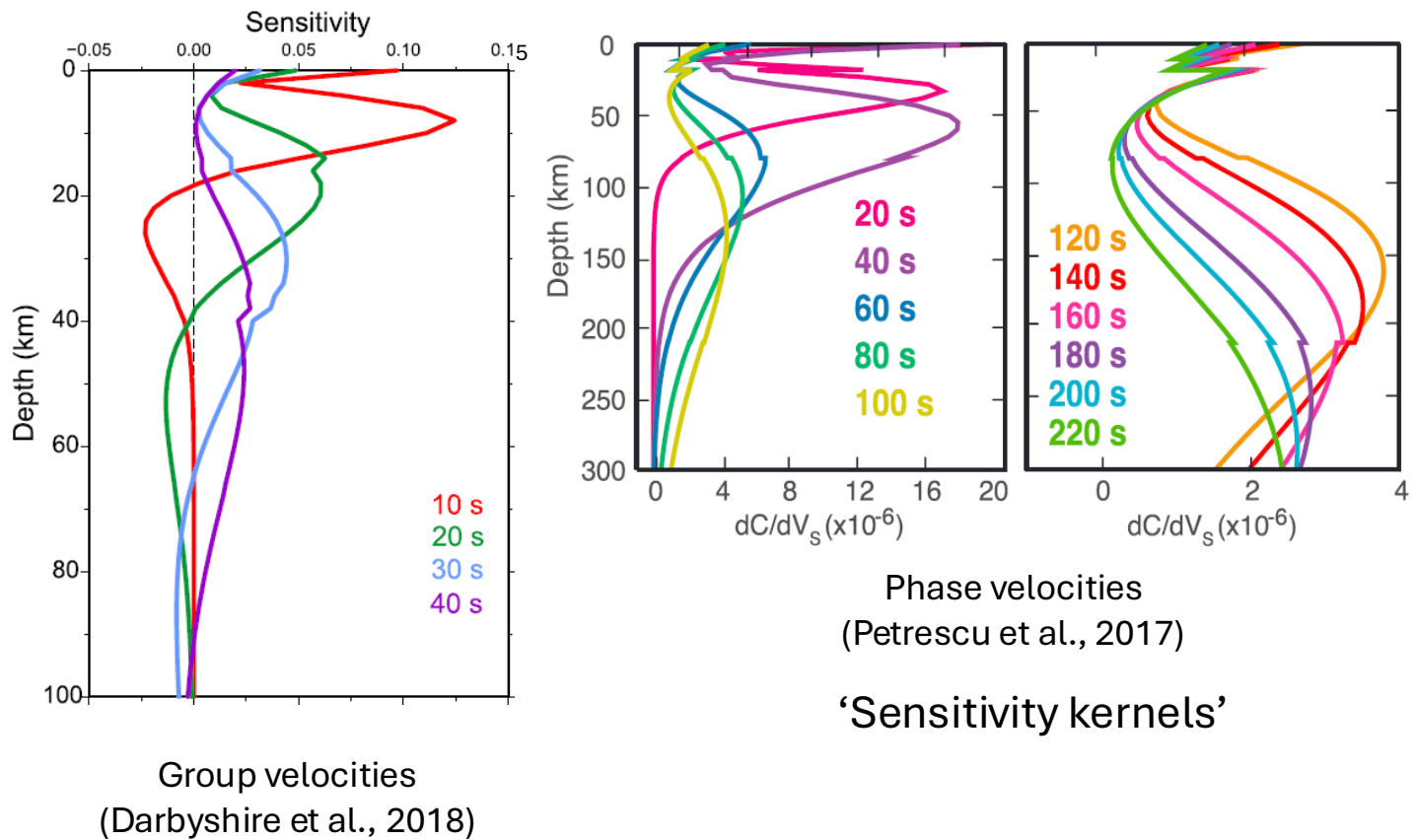
$$U = C + k \frac{dC}{dk}$$

$\omega$  – angular frequency ( $= 2\pi f$ )

$k$  – wavenumber ( $= 2\pi / \lambda$ )

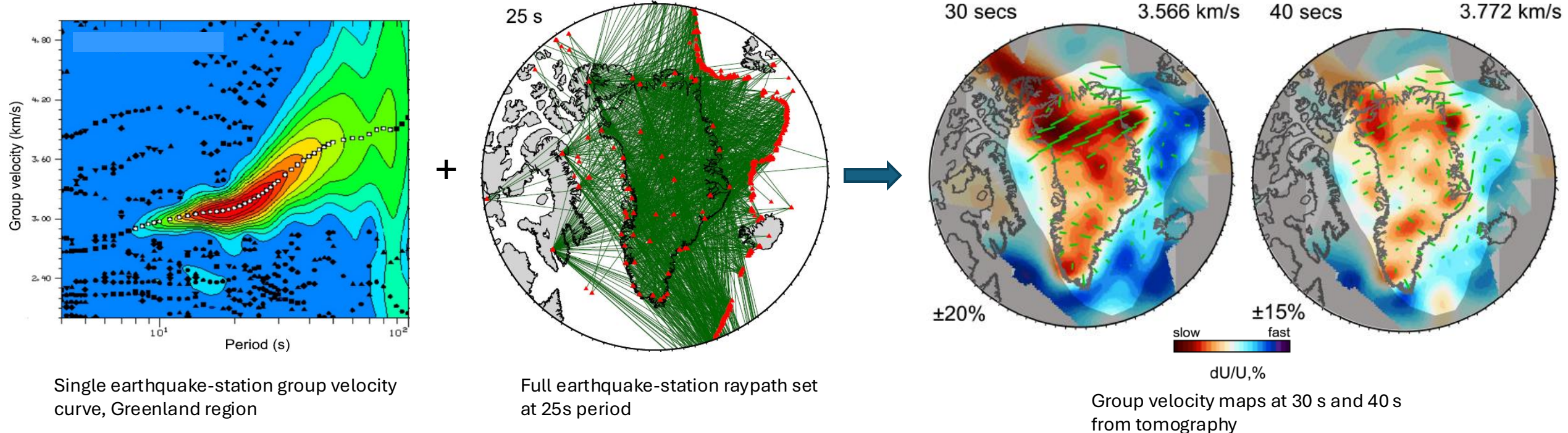
# Surface-wave tomography

- Longer wavelength (lower frequency, longer period) → deeper penetration
  - Each wave period is sensitive to a range of depths.
  - As the period increases, the depth of peak sensitivity increases, but the range of depths to which the wave is sensitive also increases.
- From surface wave velocity/period, use the sensitivity relationships to extract shear wave velocity / depth.

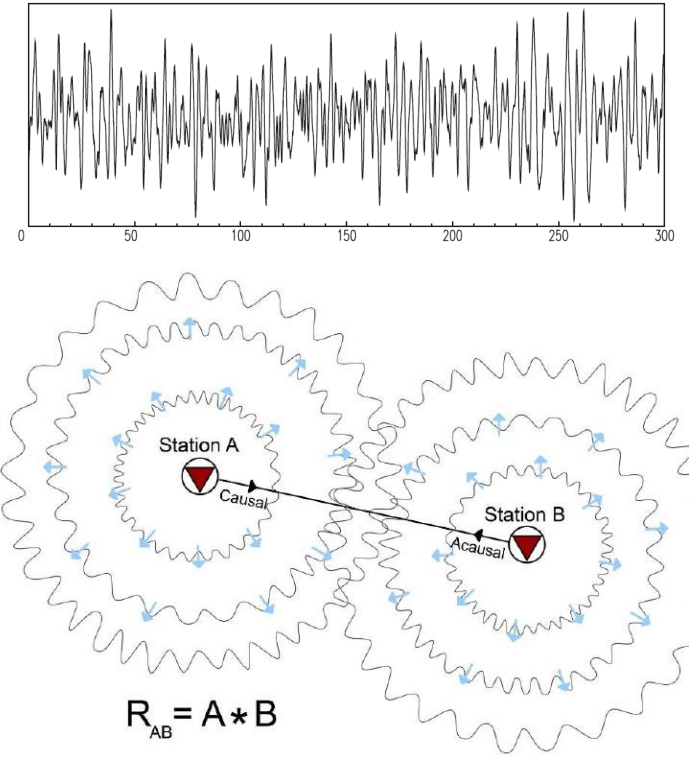


# Surface-wave tomography

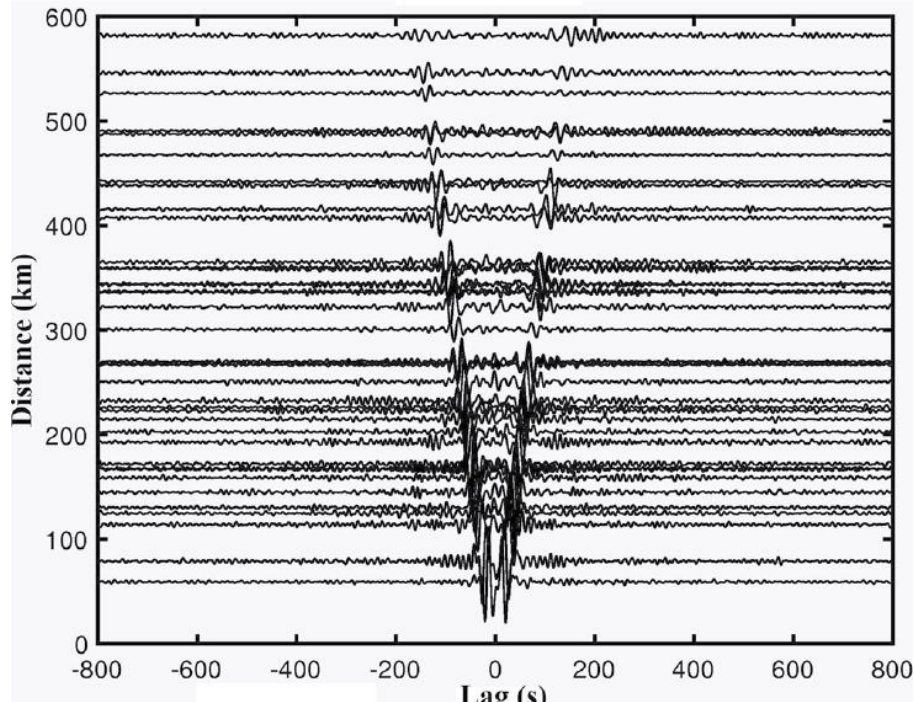
- Each surface wave dispersion curve provides information about the *average* structure along the path travelled , not lateral variations.
- Requires surface wave *tomography* to map lateral variation and (eventually) build a 3D model.
- **Strategy:** Combine multiple crossing surface wave paths → set of group or phase velocity maps (1 map per wave period analyzed)
- Can be achieved with irregular station spacing, including sparse coverage in the region of interest, as long as rays cross within this area, with good azimuthal variation.



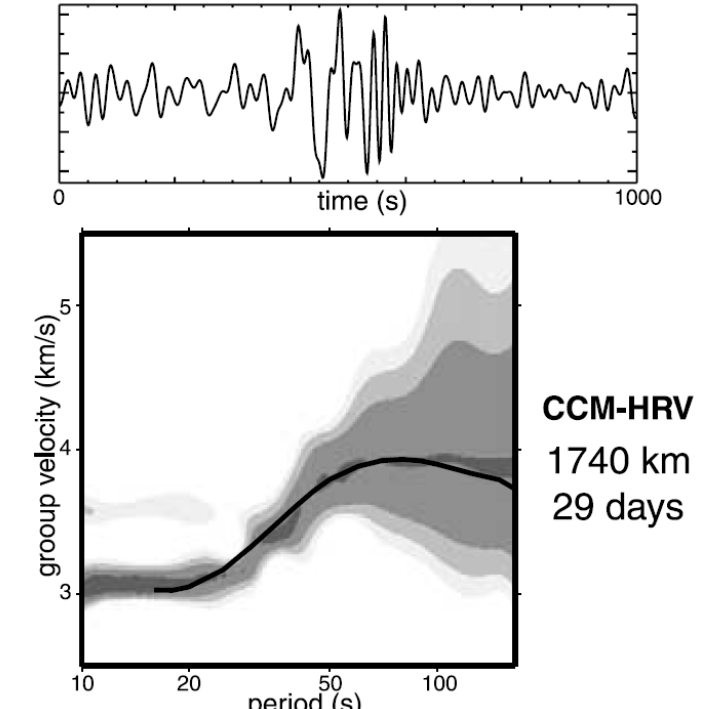
# Ambient-noise tomography (ANT)



- Seismic noise recorded by a single station appears random... but cross-correlation of noise between two stations yields the inter-station Empirical Green's Function... which can be analyzed exactly like a surface wave.



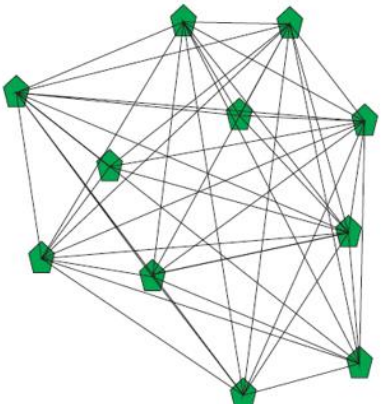
- Cross-correlation of vertical-component energy yields ~Rayleigh waves at both positive (B to A) and negative (A to B) lags.
- Note the moveout for increasing inter-station distances.
- The resulting waveforms yield group and phase velocity dispersion curves.
- Due to typical frequency content and inter-station distances, most dispersion is well resolved in the ~5-40 s period range.



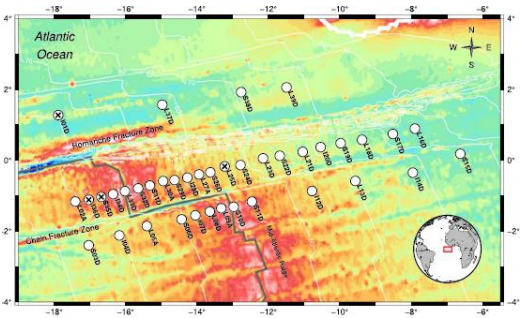
# Ambient-noise tomography (ANT)

Advantages of ambient noise analysis:

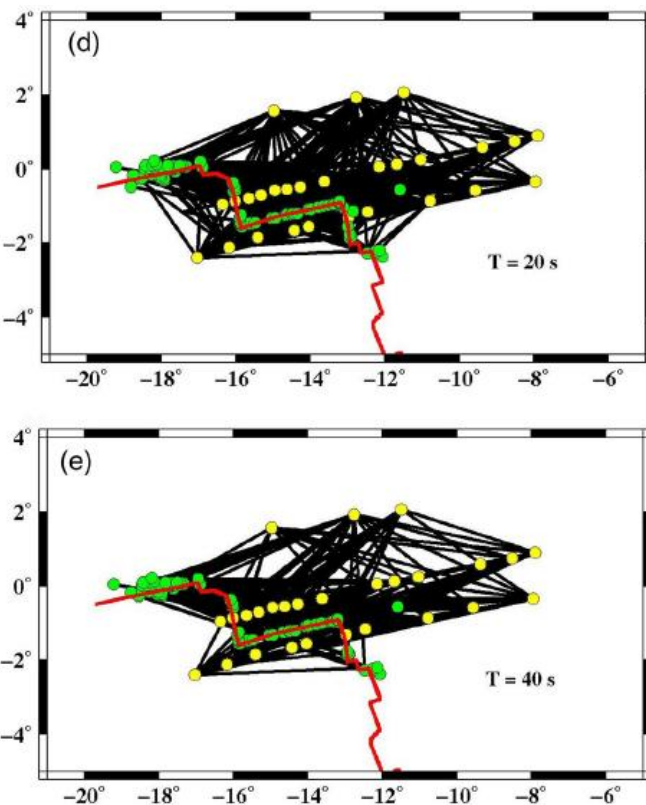
- Path coverage: all station pairs
- No need for seismic sources – can use just a few months of noise data



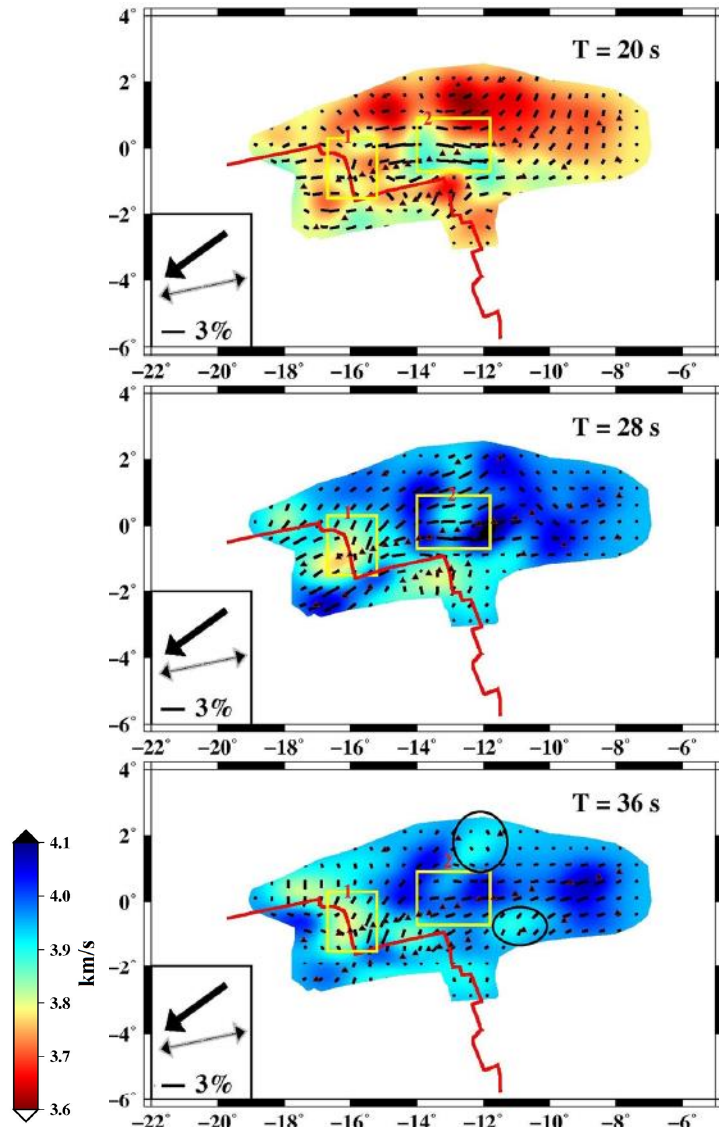
Ambient-noise data set  
– **ALL** paths possible



*PI-LAB* raypaths from ambient noise cross-correlations and local earthquakes



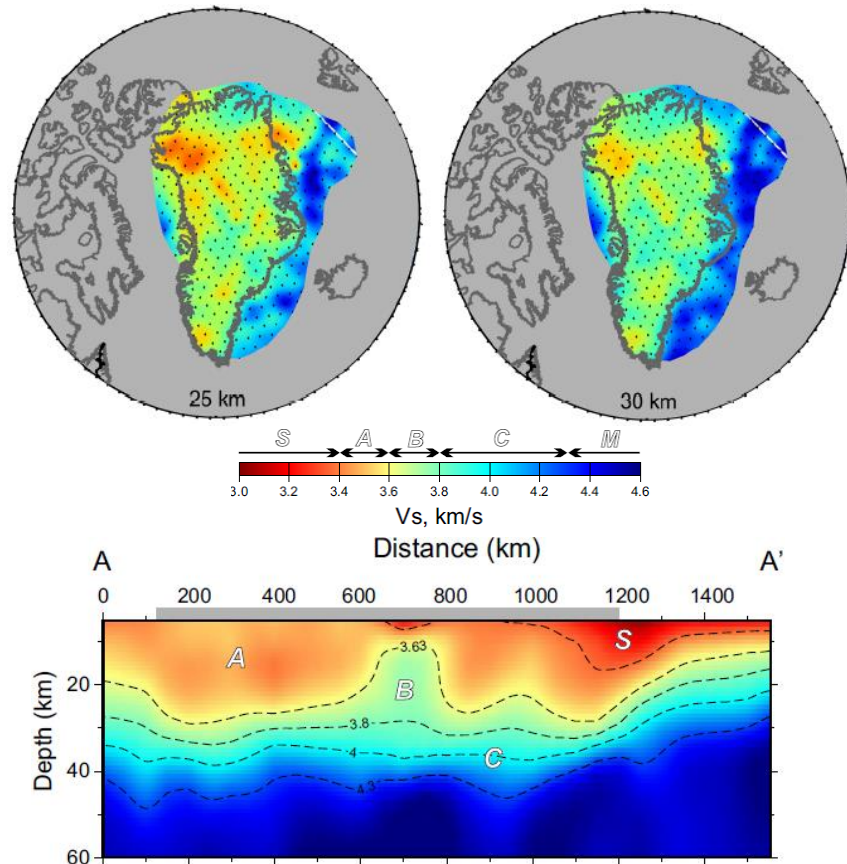
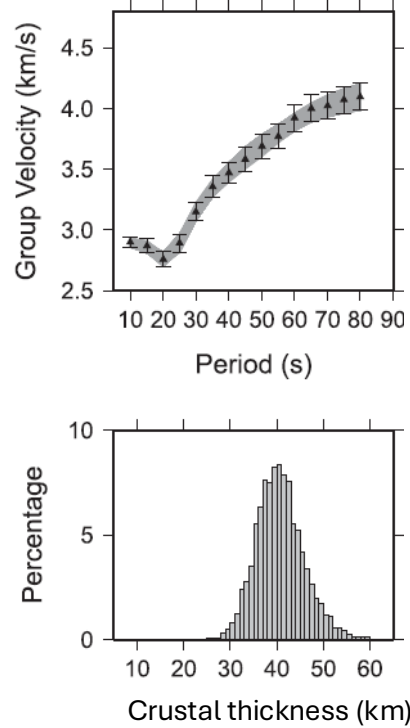
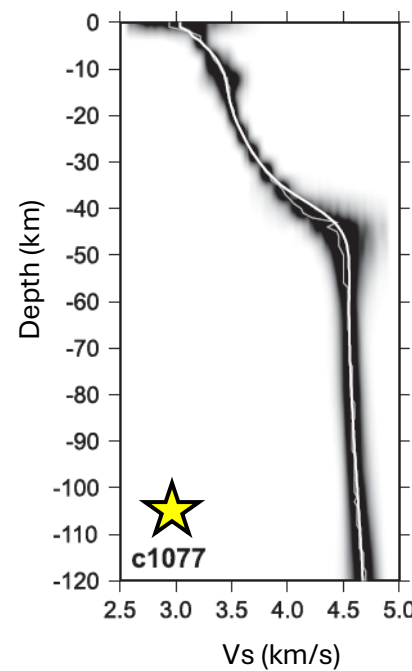
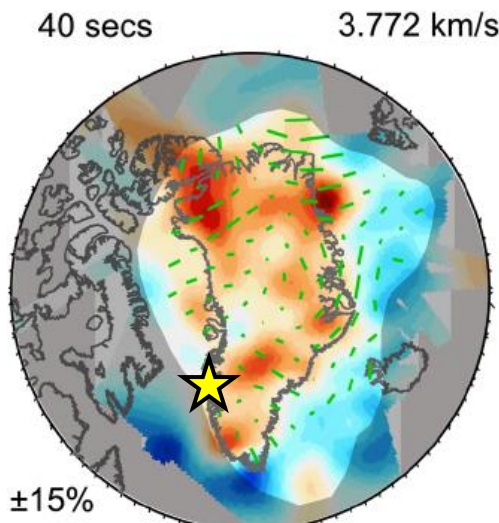
Saikia et al. (2021)



*PI-LAB* group velocity maps

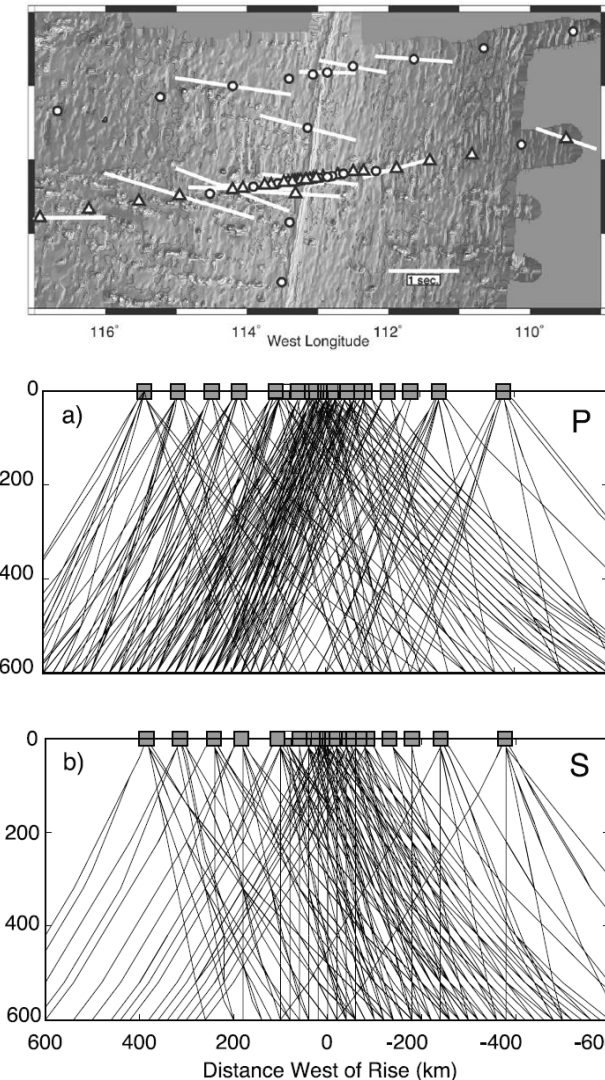
# Surface-wave tomography

- From the group or phase velocity maps:
- Extract phase velocity at each grid node for all periods → new dispersion curve representing 1D structure at a given latitude/longitude
- Invert dispersion curve to obtain a 1D profile of shear wave velocity vs. depth, using known sensitivity functions
- Interpolate results → (pseudo-) 3D model



# Resolution

- Model *resolution tests* are very important due to uneven source distribution, ray geometry, smearing of structure along ray paths, and other possible artefacts.
- Need to know what structures in the model can be considered reliable and what is the smallest resolvable structure.
- Standard methods:
  - Basic ray coverage diagrams
  - Checkerboard tests
  - Structural tests
- For checkers and structures:
  - Create an artificial model with fast and slow anomalies
  - Trace rays through the model using the same source-receiver geometry
  - Add random noise → synthetic data set,
  - Invert the synthetic data using the same parameters as the real data
  - See how well the artificial model is recovered.

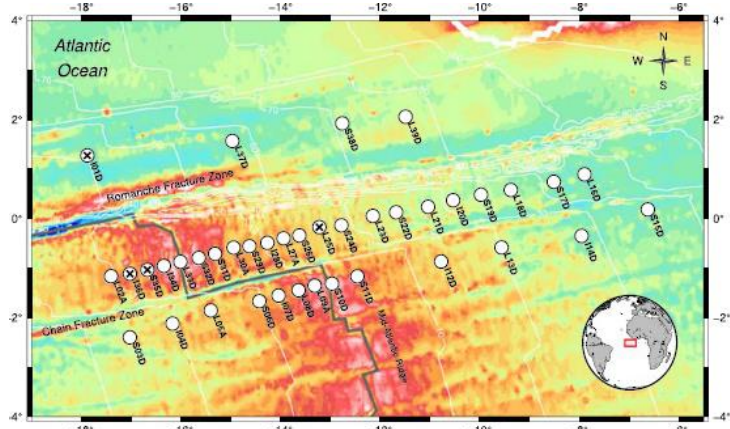


MELT experiment, East Pacific Rise  
Array aperture ~800 x 300 km  
Body-wave tomography



Hammond & Toomey (2003)

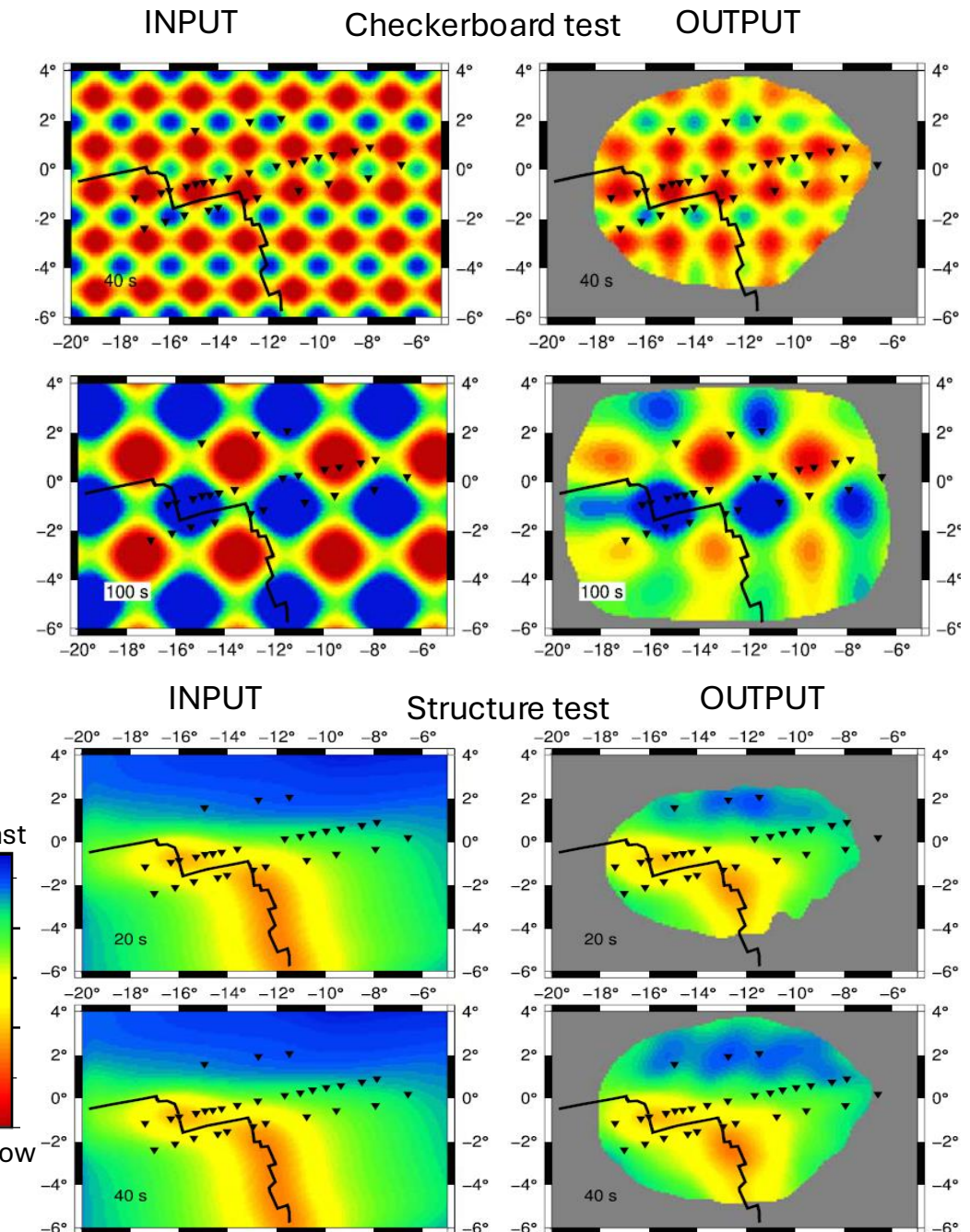
# Resolution



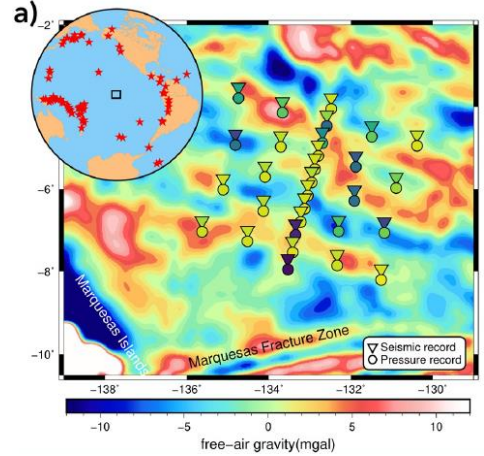
- *PI-LAB* experiment, central-southern Mid-Atlantic Ridge
- Array aperture  $\sim 1200 \times 450$  km
- Surface wave and ambient-noise tomography

Resolution tests applied to phase velocity maps → information only on lateral resolution

Harmon et al. (2020)



# Resolution

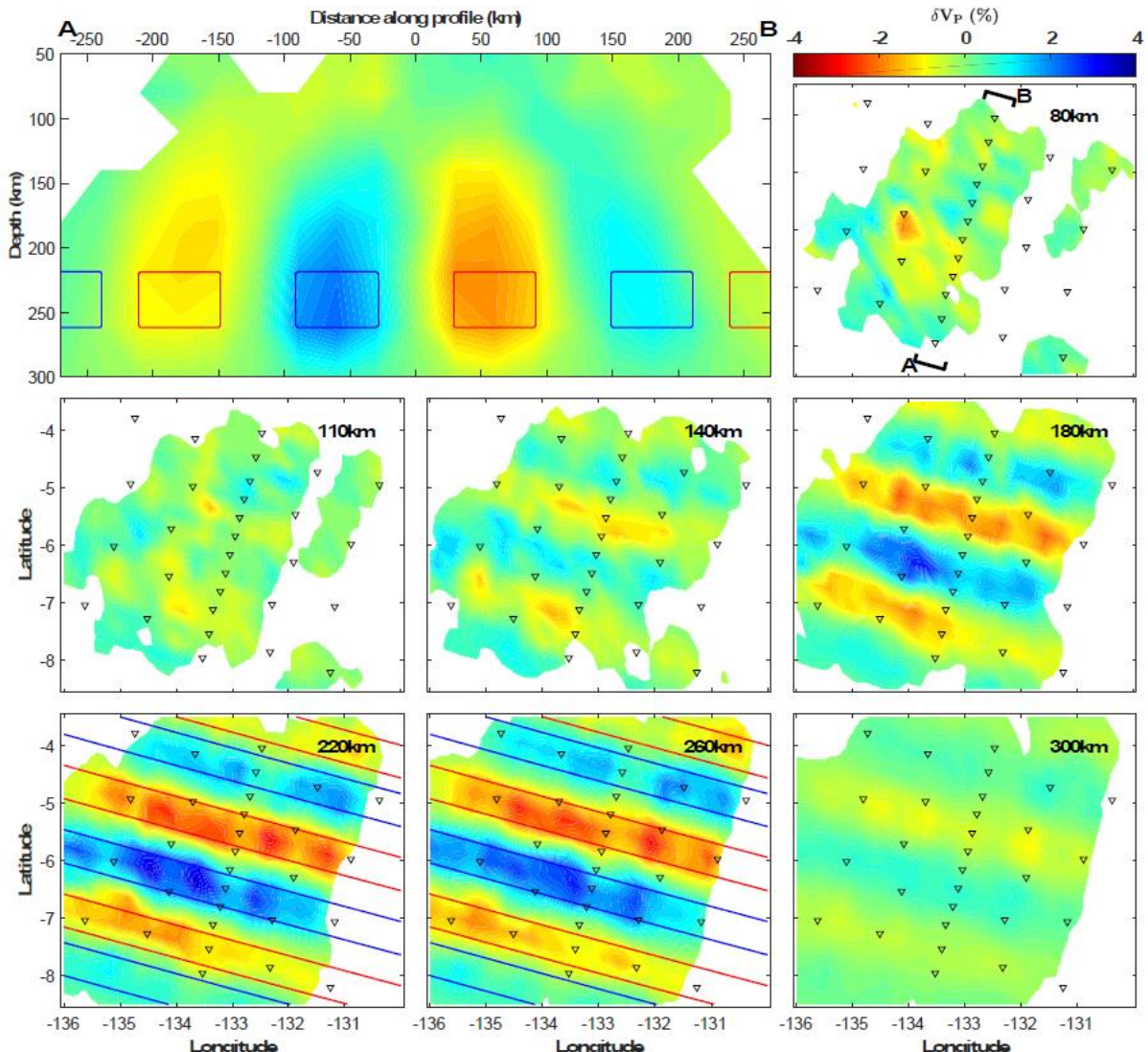


- ORCA experiment, mid-Pacific Ocean
- Network aperture  $\sim 500 \times 500$  km
- Body wave tomography

Eilon et al. (2022)

Resolution tests applied to 3D tomographic model  
→ information on lateral & vertical resolution

Note good lateral resolution but strong *vertical smearing* – deep structures are often smeared upwards from the model base; shallower structures are often smeared downwards.

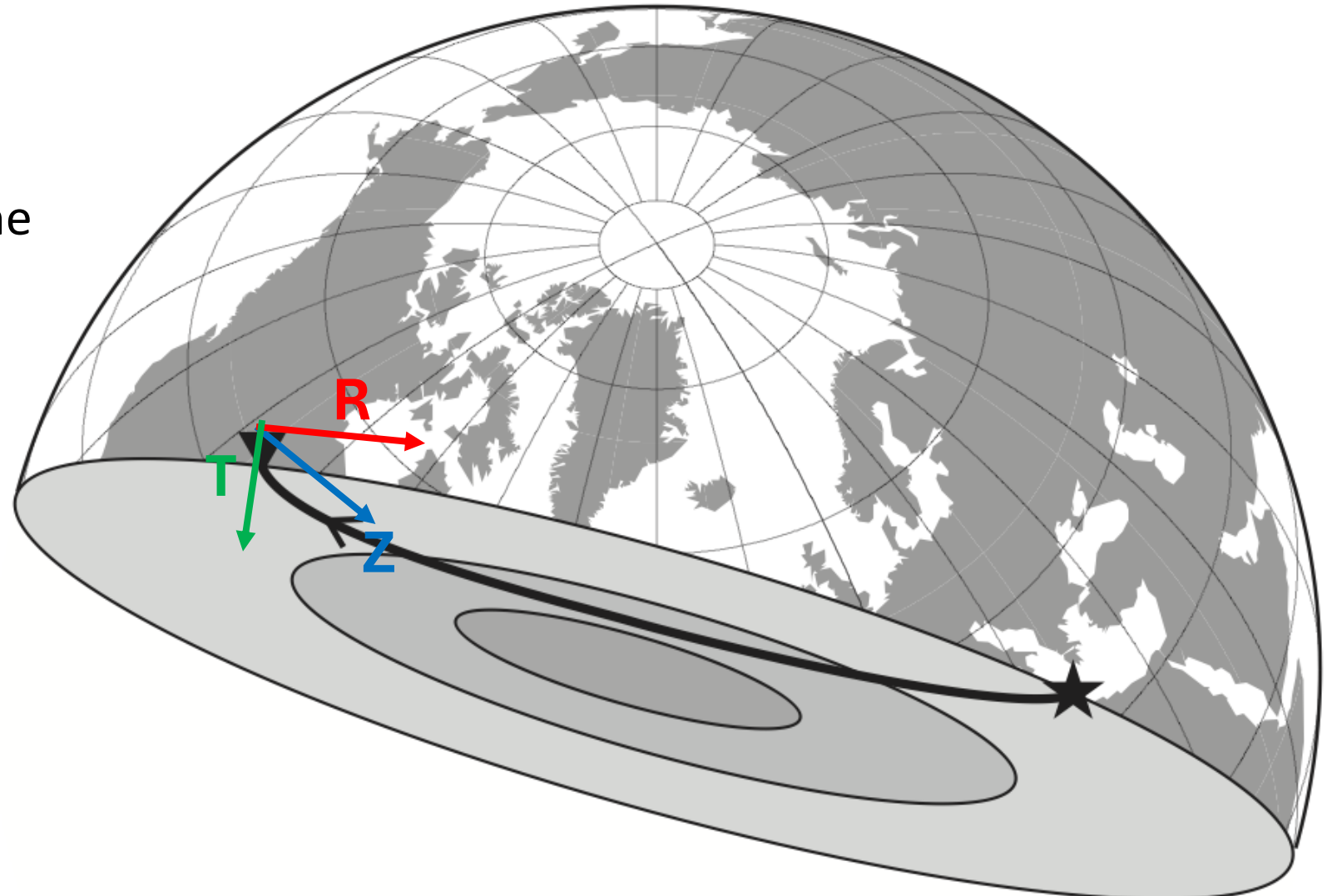


# Receiver functions: General principles

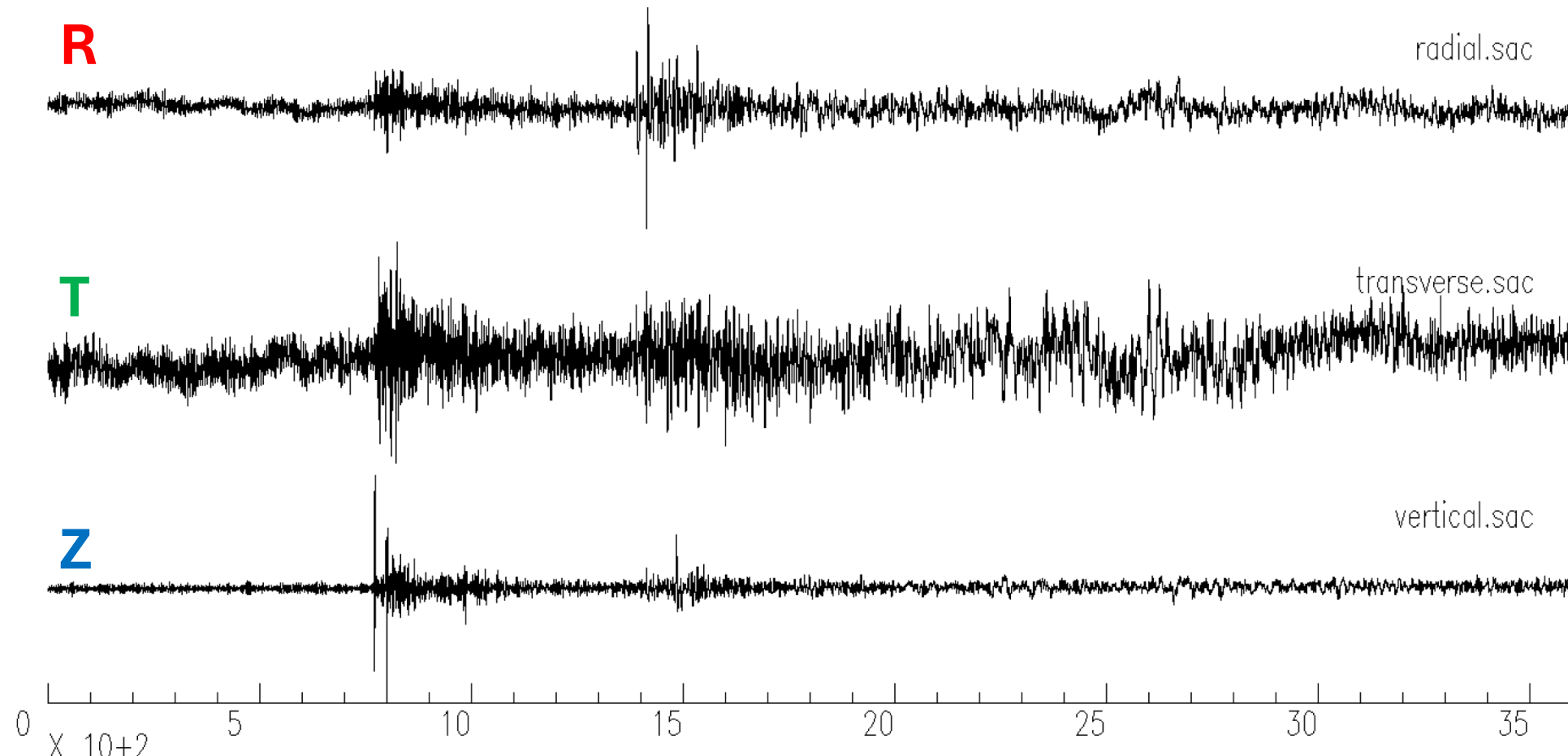
Radial: horizontal, in ray plane

Transverse: horizontal,  
perpendicular to ray plane

Vertical: in ray plane

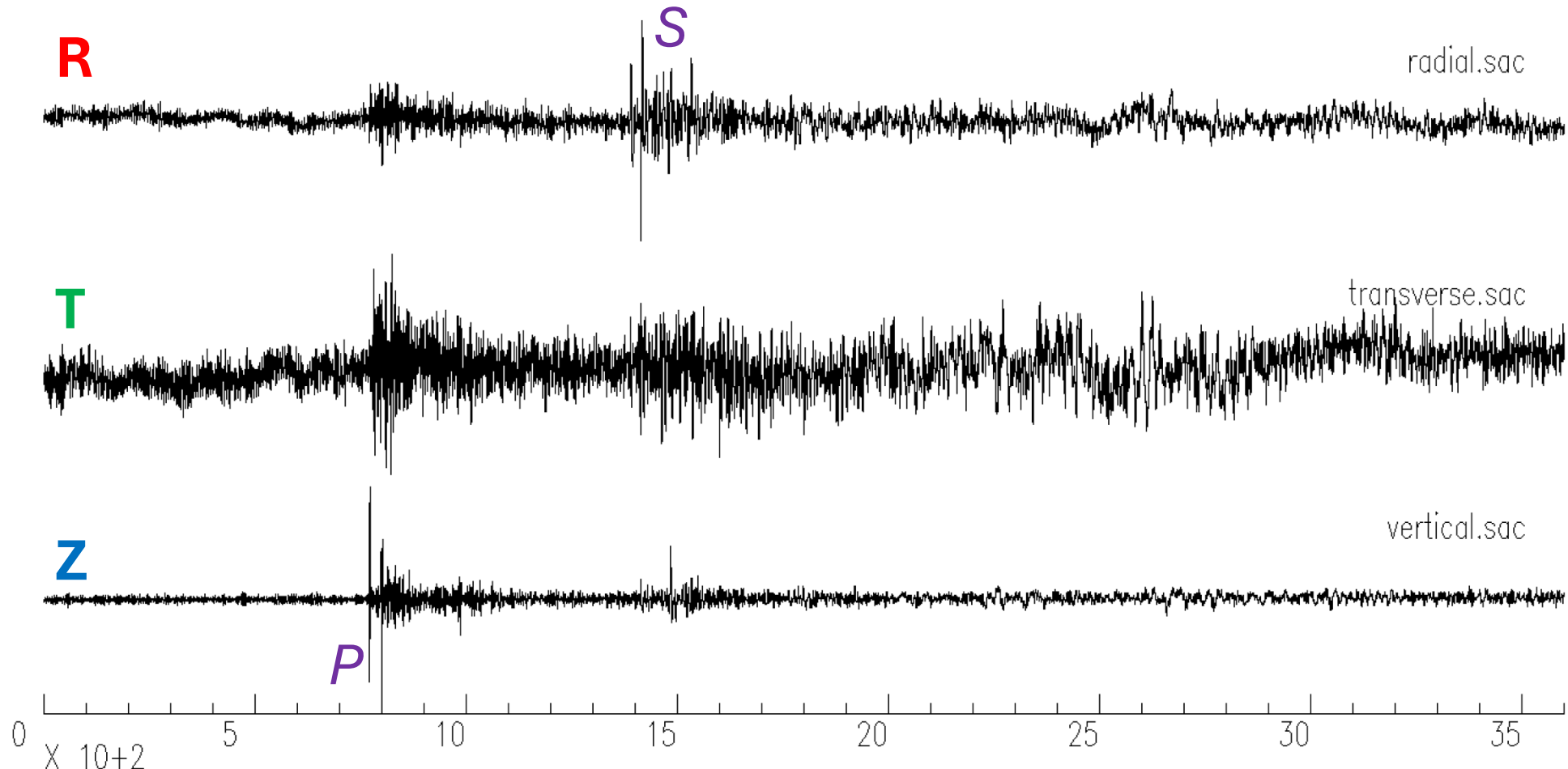


# Receiver functions: General principles



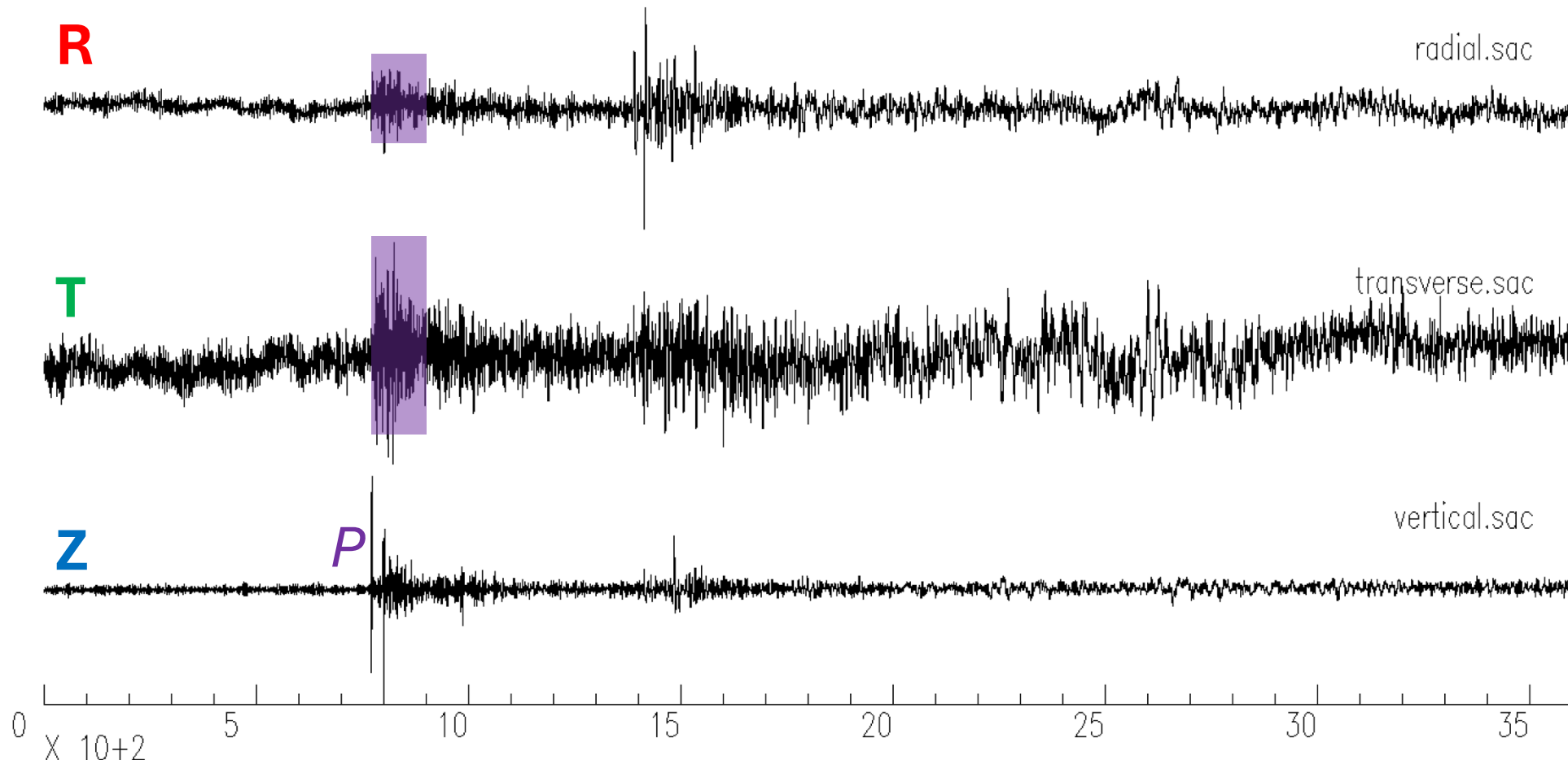
Here's how three-component seismic data look in this coordinate system. This earthquake was 90° away from the receiver and 130 km deep.

# Receiver functions: General principles



Note how the arrivals have different polarizations – P is largely vertical, S is largely radial. The transverse looks noisy because it's lower amplitude than the other components.

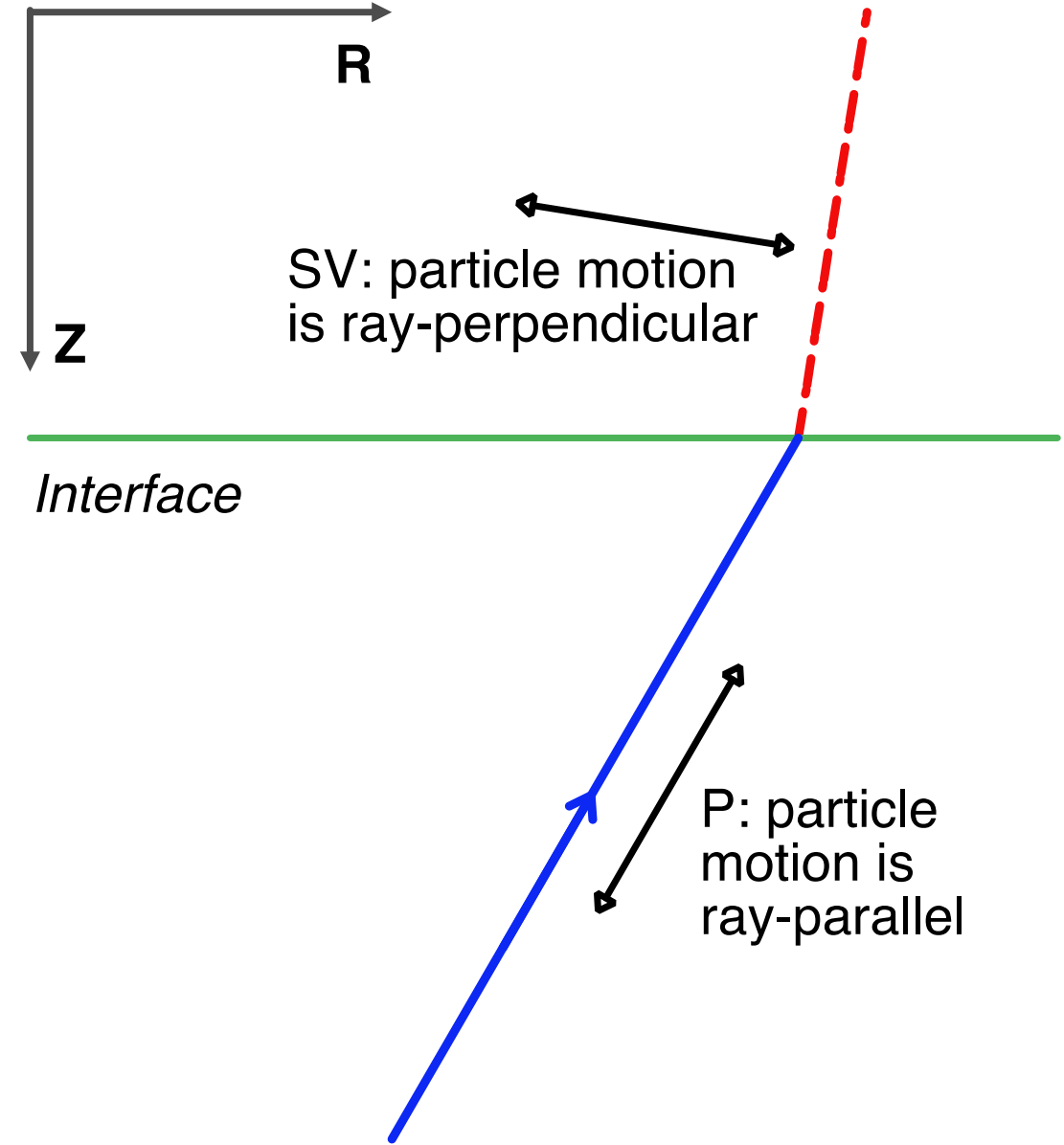
# Receiver functions: General principles



To understand **receiver functions**, note how the P pulse is followed by a *coda*, particularly on the horizontal components.

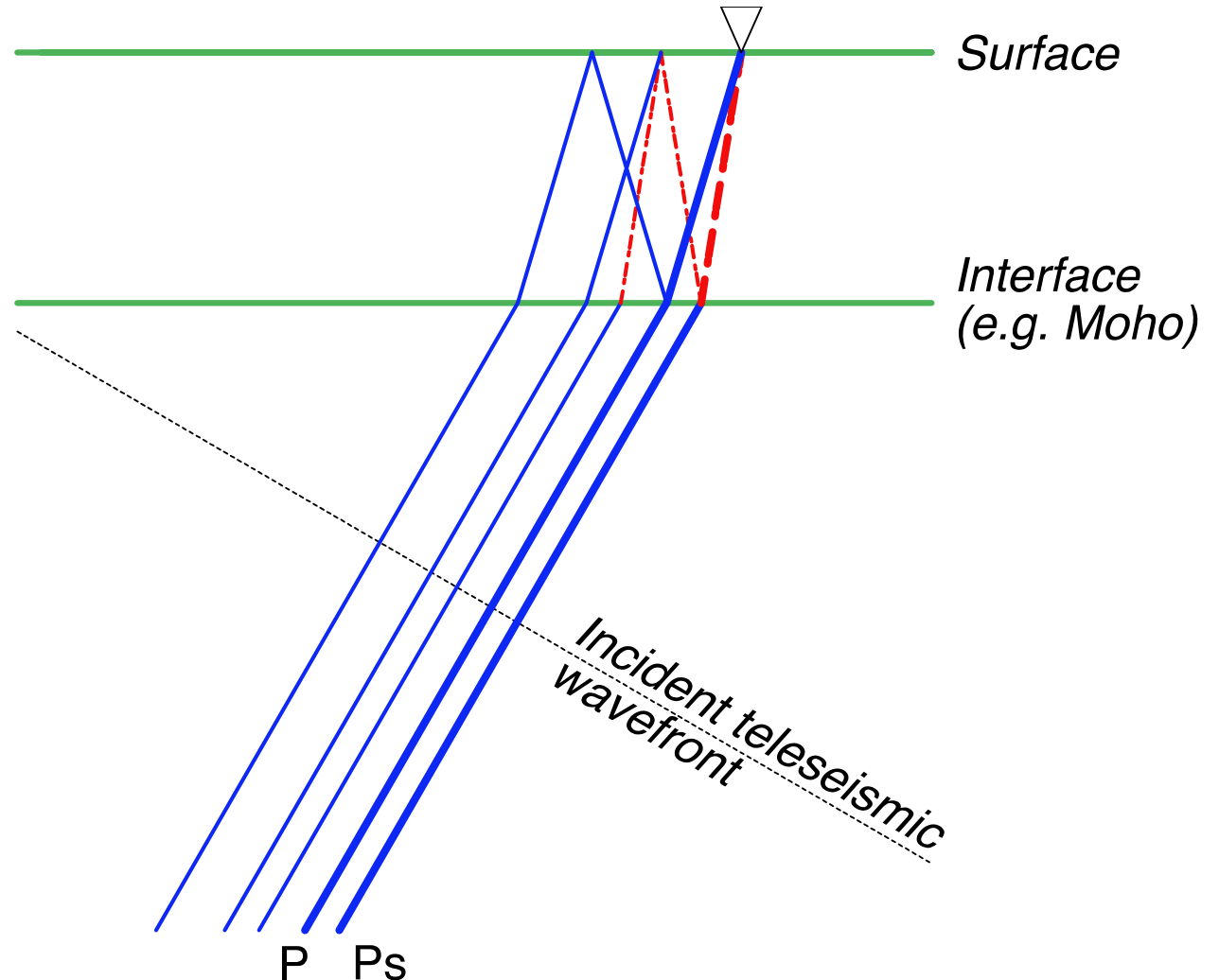
# Receiver functions

- The additional horizontal coda energy largely comes from *converted* waves.
- At a sharp interface, some of the incident energy will convert from one wave mode to another.
- If the incident wave is P, the converted S wave will be SV polarized (if the interface is horizontal and the medium is isotropic).
- At *teleseismic* distances (30-100°, where the P arrival is clean), the incident ray is steeply angled, so the P energy is largely vertical and the Ps converted energy is largely radial.



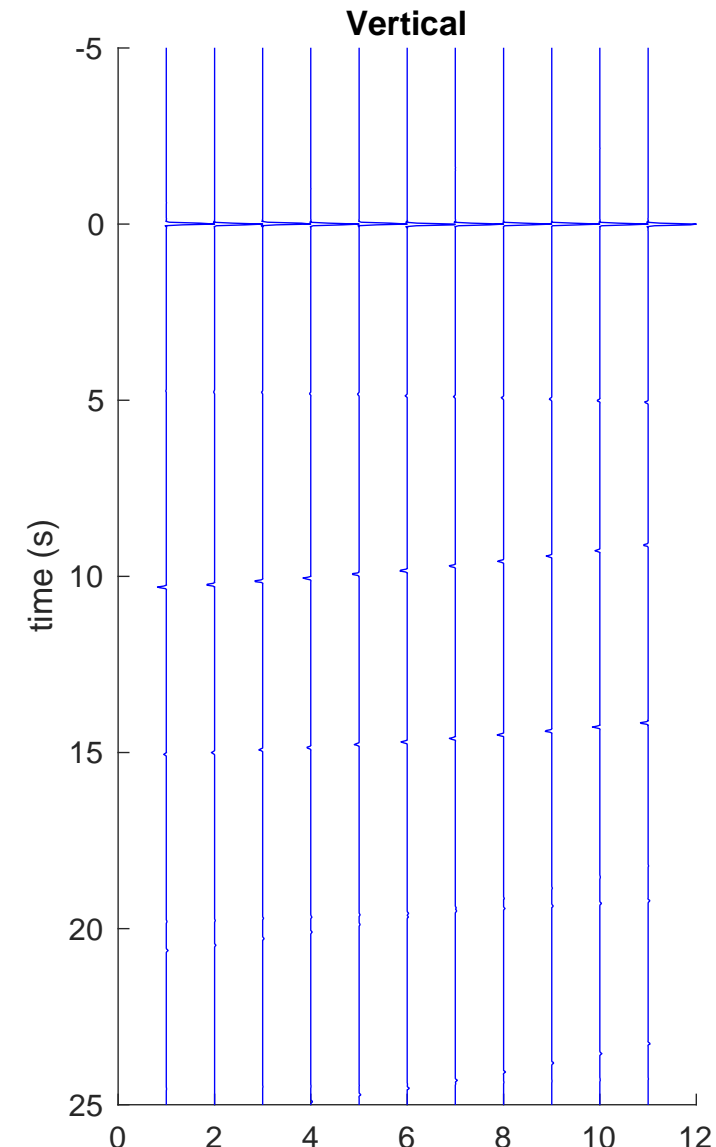
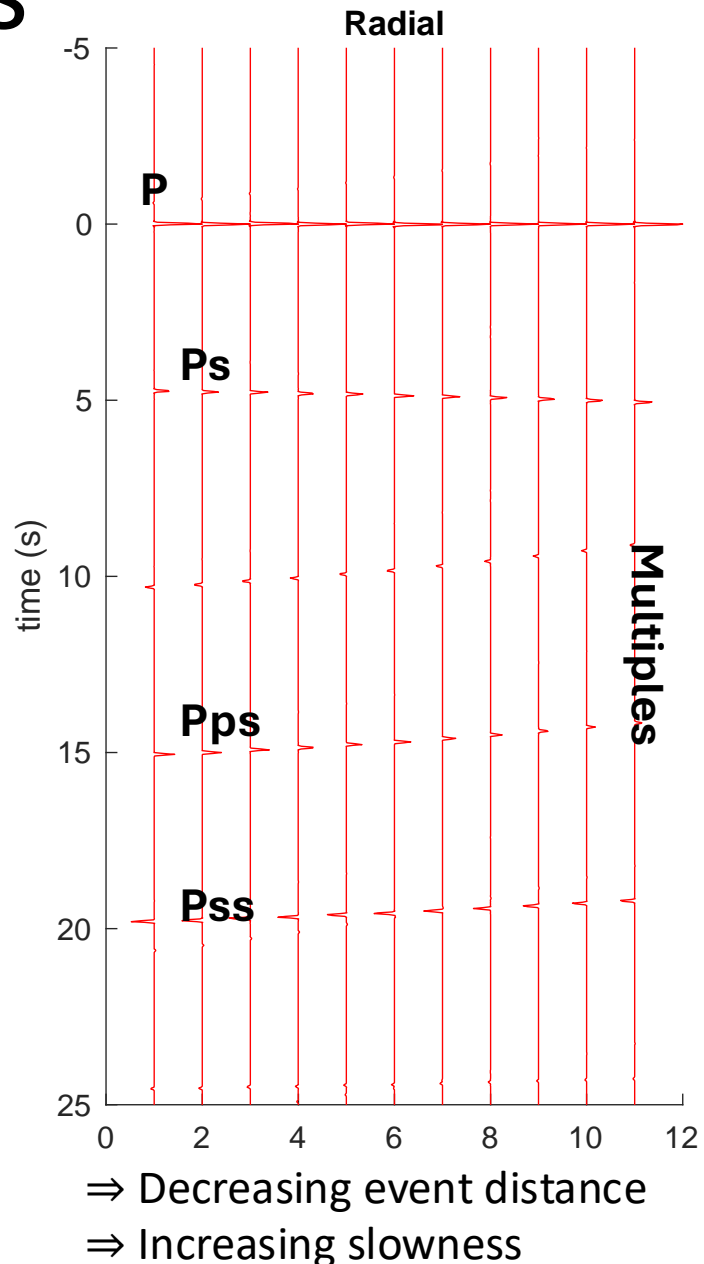
# Receiver functions

- The P coda will contain both Ps conversions and reverberations – much like the primary reflections and multiples seen in reflection data.
- The Ps conversions are the most commonly used source of information in a receiver function, but the multiples ( $P_{ps} + P_{ss}$ ) are also used to characterize strong interfaces like the Moho.



# Receiver functions

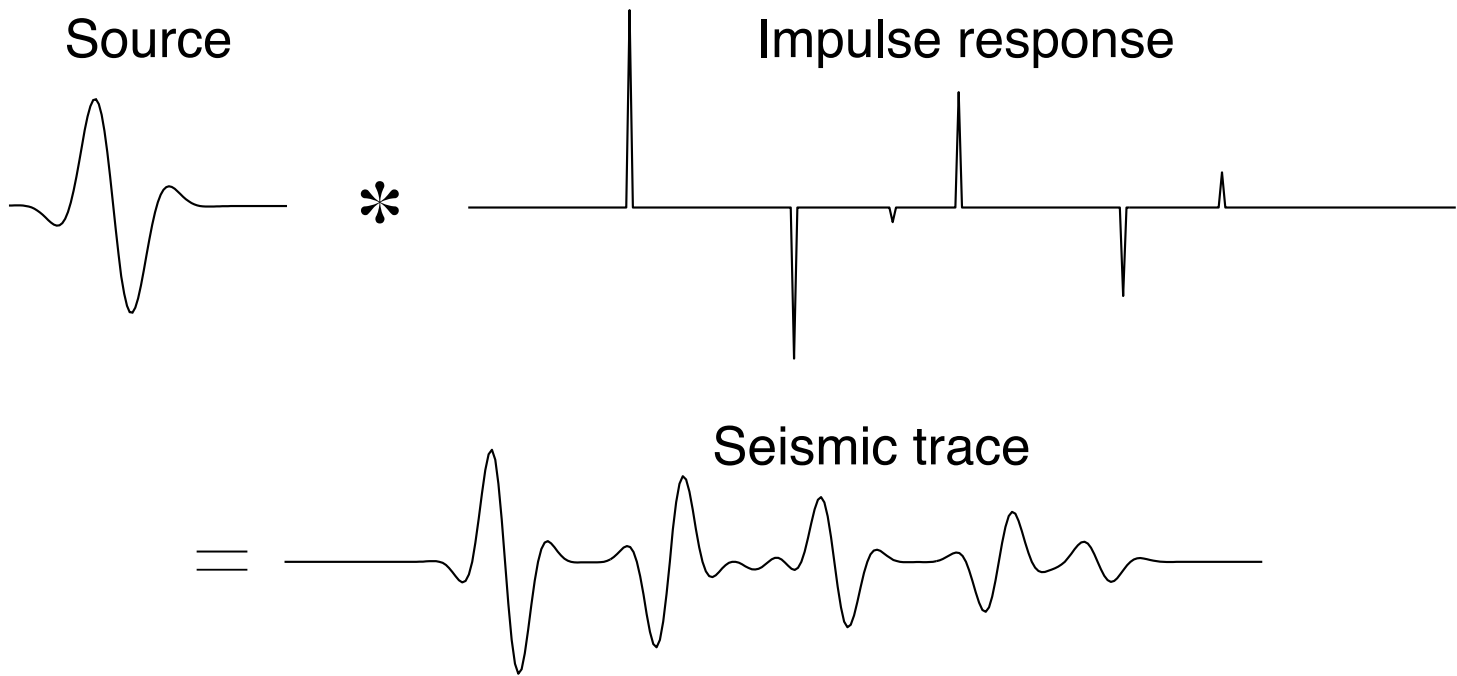
- “Ideal” seismograms of these arrivals will look like this (for a 35 km Moho and a single-layer crust).
- But real data will be (1) much lower frequency than this, and (2) overlain with a source waveform.
- If the source waveform is more than, say, 5 seconds long, the P and Ps arrivals will overlap!
- Thus, to use raw data for this, we’d only be able to use a few deep earthquakes.



# Receiver functions

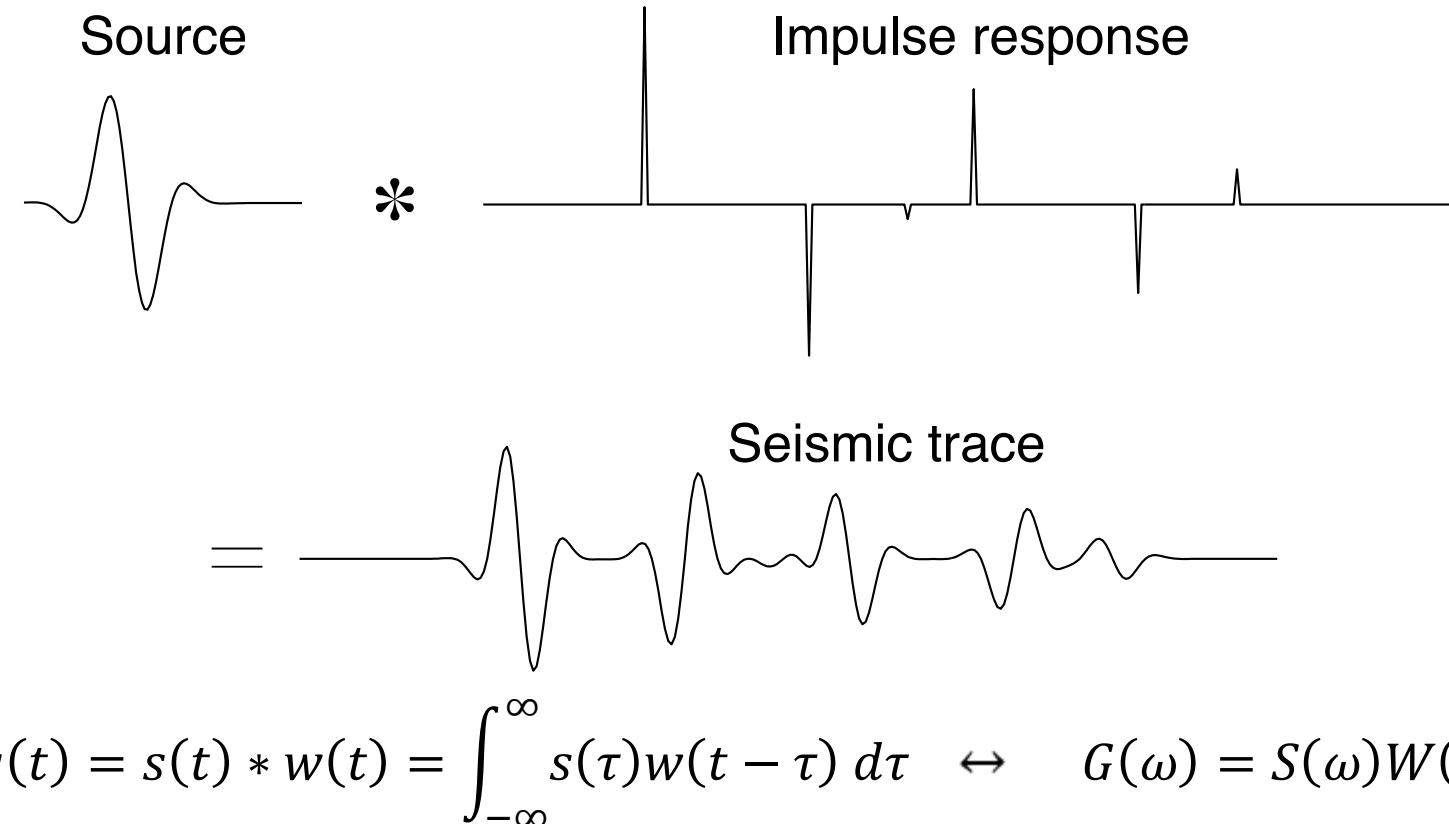
- The seismic trace  $g(t)$  we record is the *convolution* of the source waveform  $s(t)$  with an impulse response  $w(t)$  representing the effect of structure. This is written as an integral:

$$g(t) = s(t) * w(t) = \int_{-\infty}^{\infty} s(\tau)w(t - \tau) d\tau$$



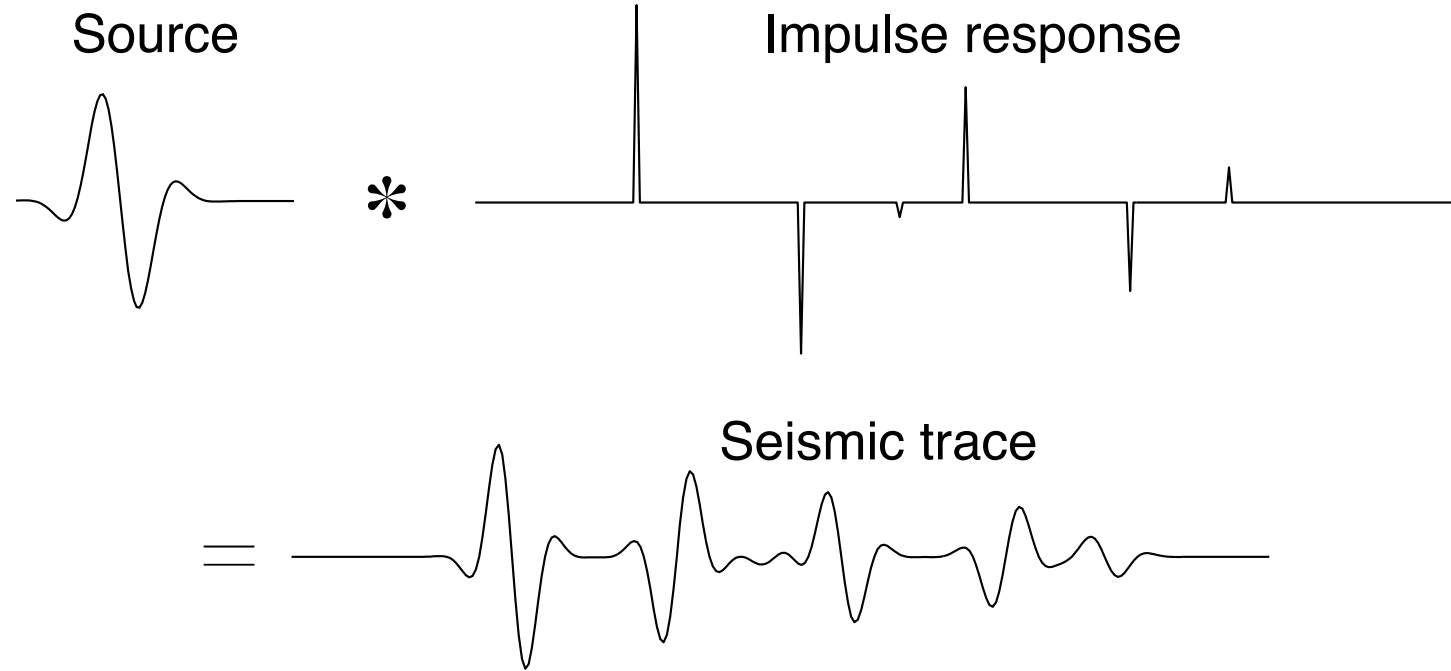
- The result of this convolution is that every arrival is a scaled repetition of the source.

# Receiver functions



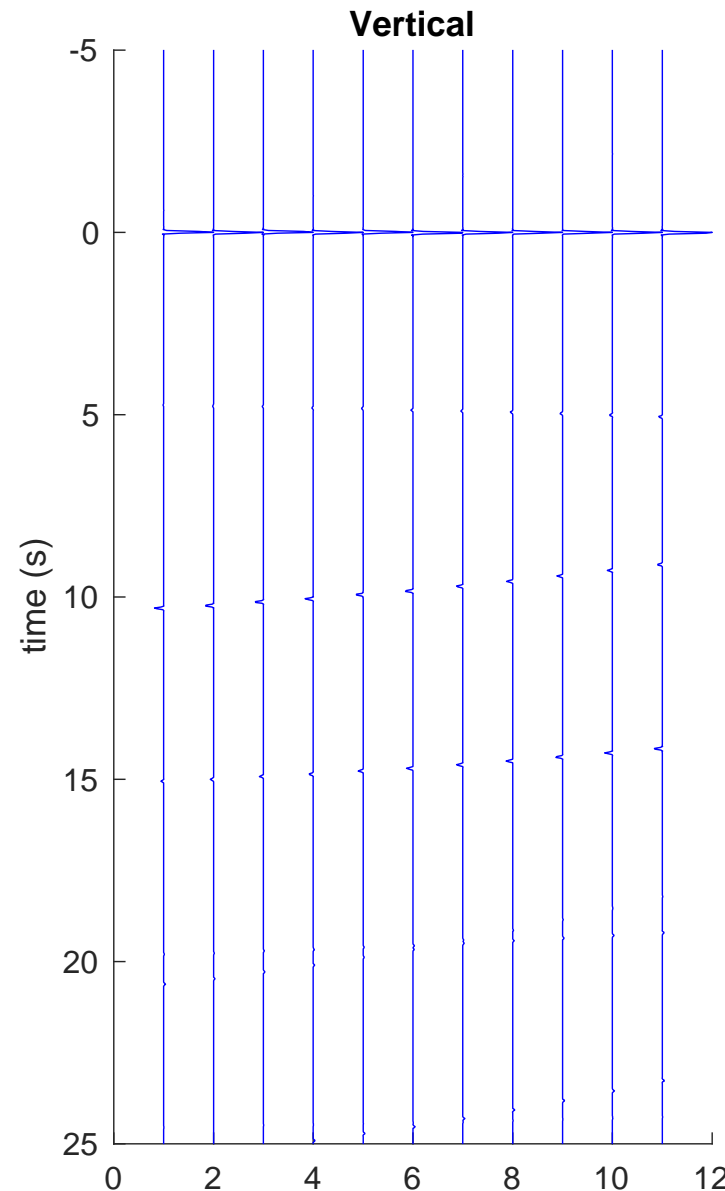
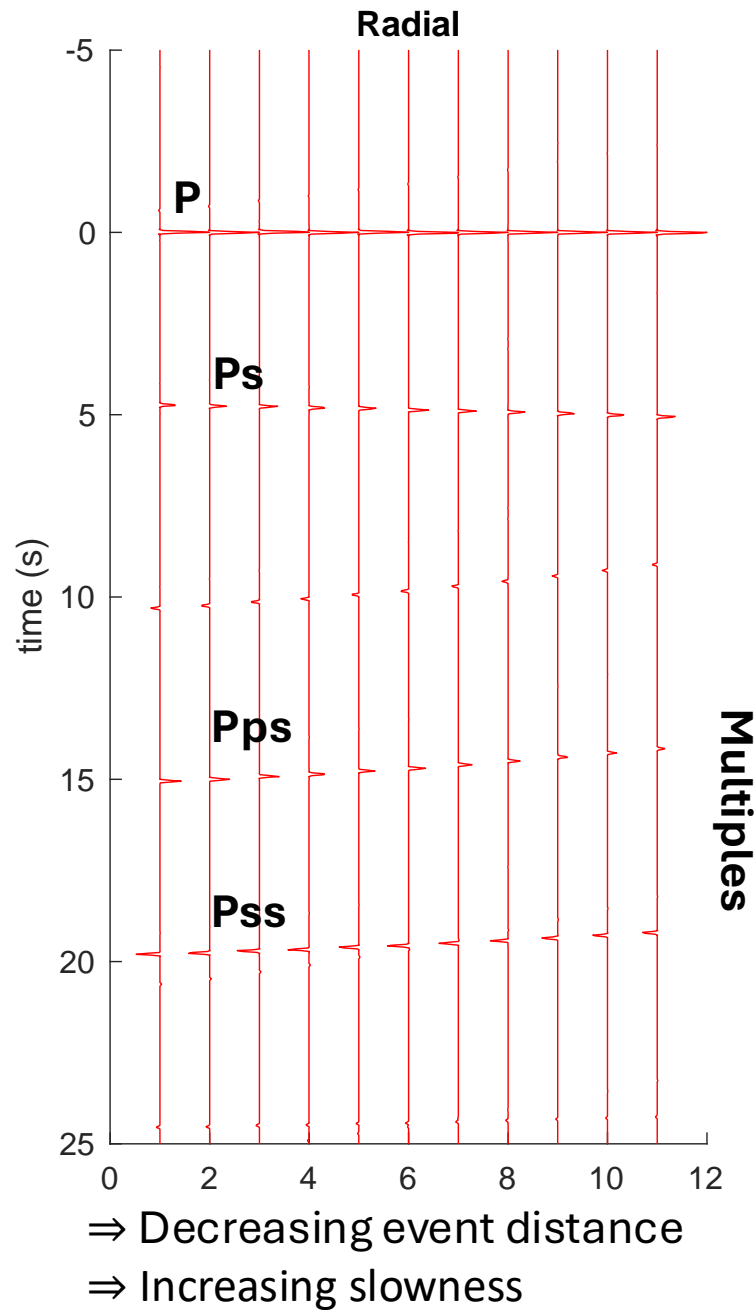
- In the frequency domain, convolution is a *spectral product* – that is, any frequency present in both the source and the impulse response will be present in the data. But any frequency missing in the source will not, except as noise – it's impossible to recover frequencies that aren't in the source pulse.

# Receiver functions



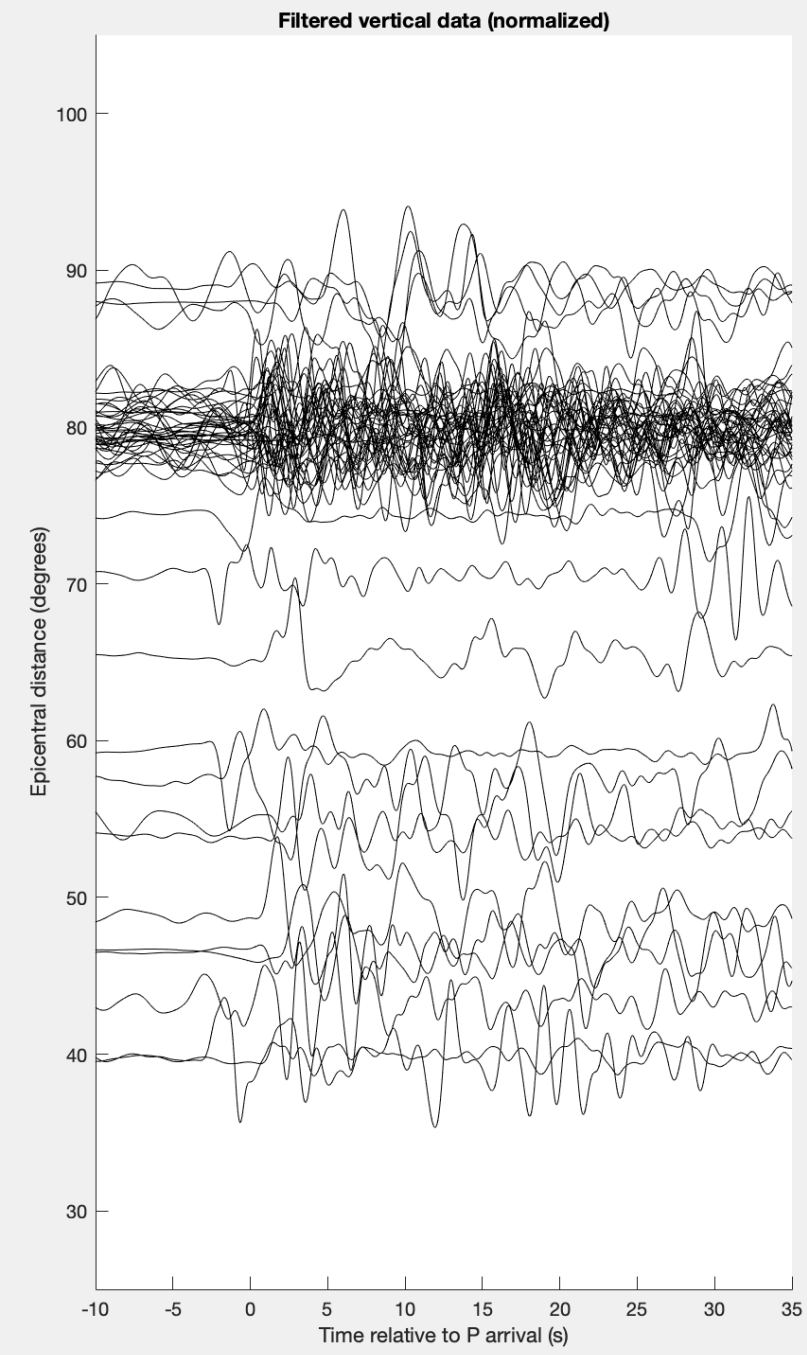
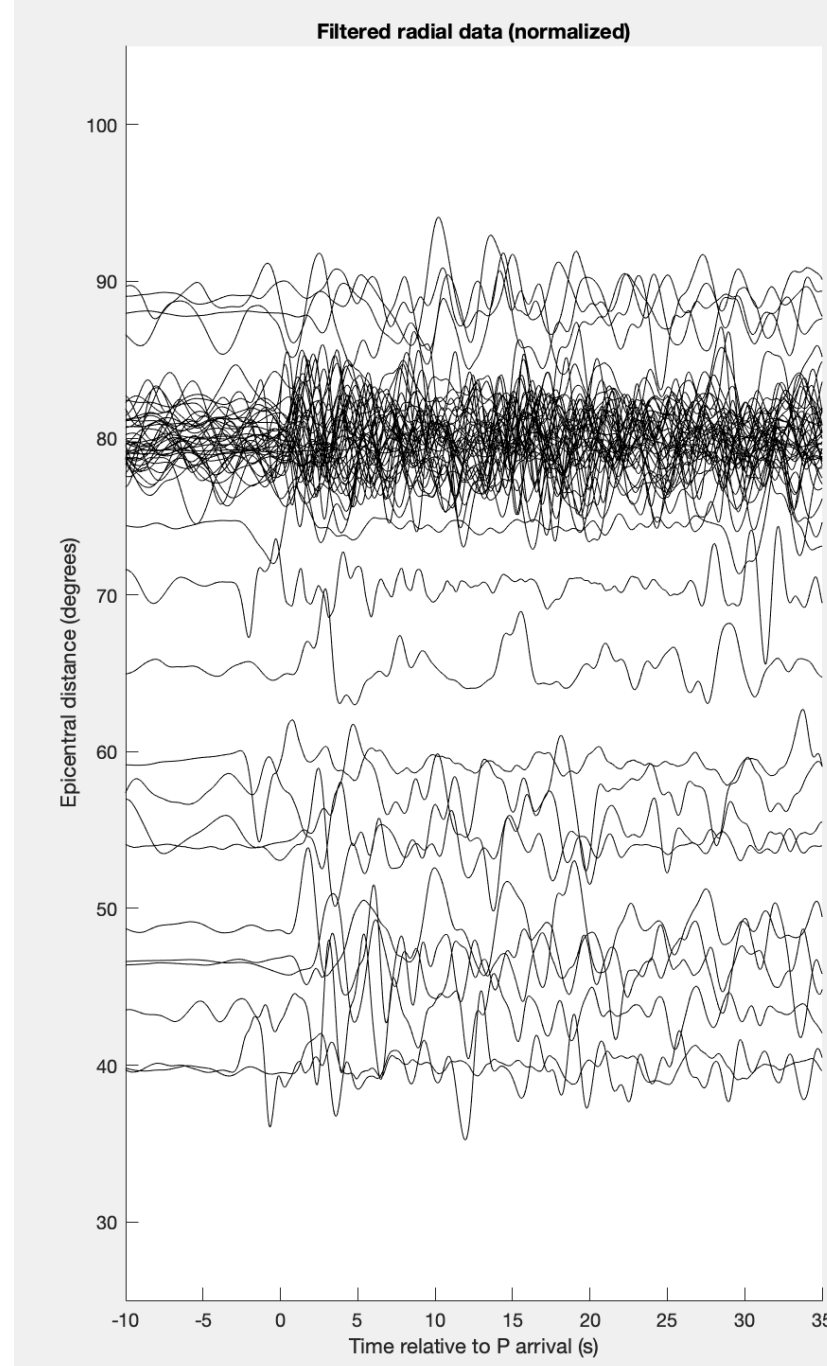
$$G(\omega) = S(\omega)W(\omega) \quad \text{so} \quad W(\omega) \approx \frac{G(\omega)S^*(\omega)}{S(\omega)S^*(\omega) + \delta}$$

- So to recover the impulse response, we need to perform a *deconvolution*, recovering the impulse response within the limits of the available frequencies. There are a number of algorithms for this (which I won't go into). Note that to deconvolve, you need an estimate of the source time function!

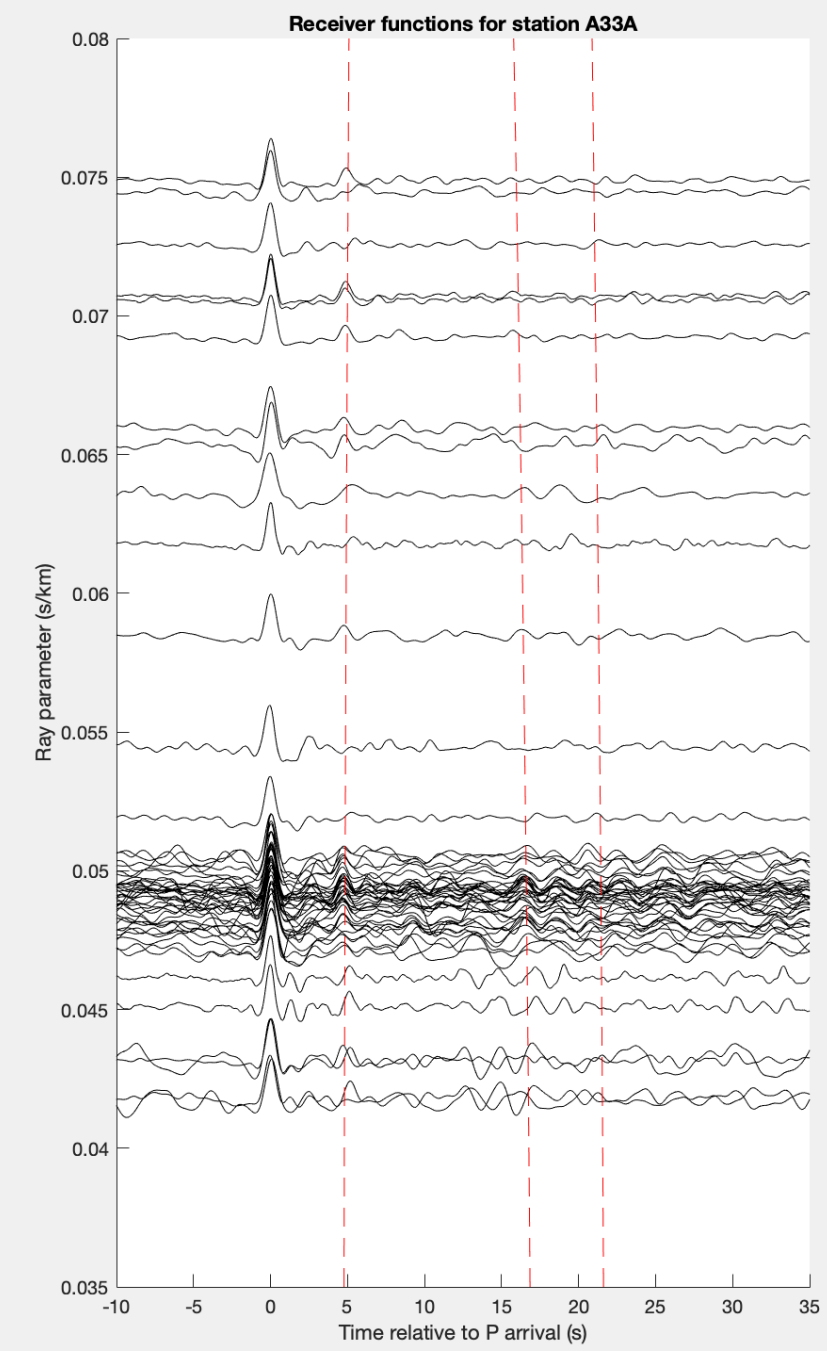
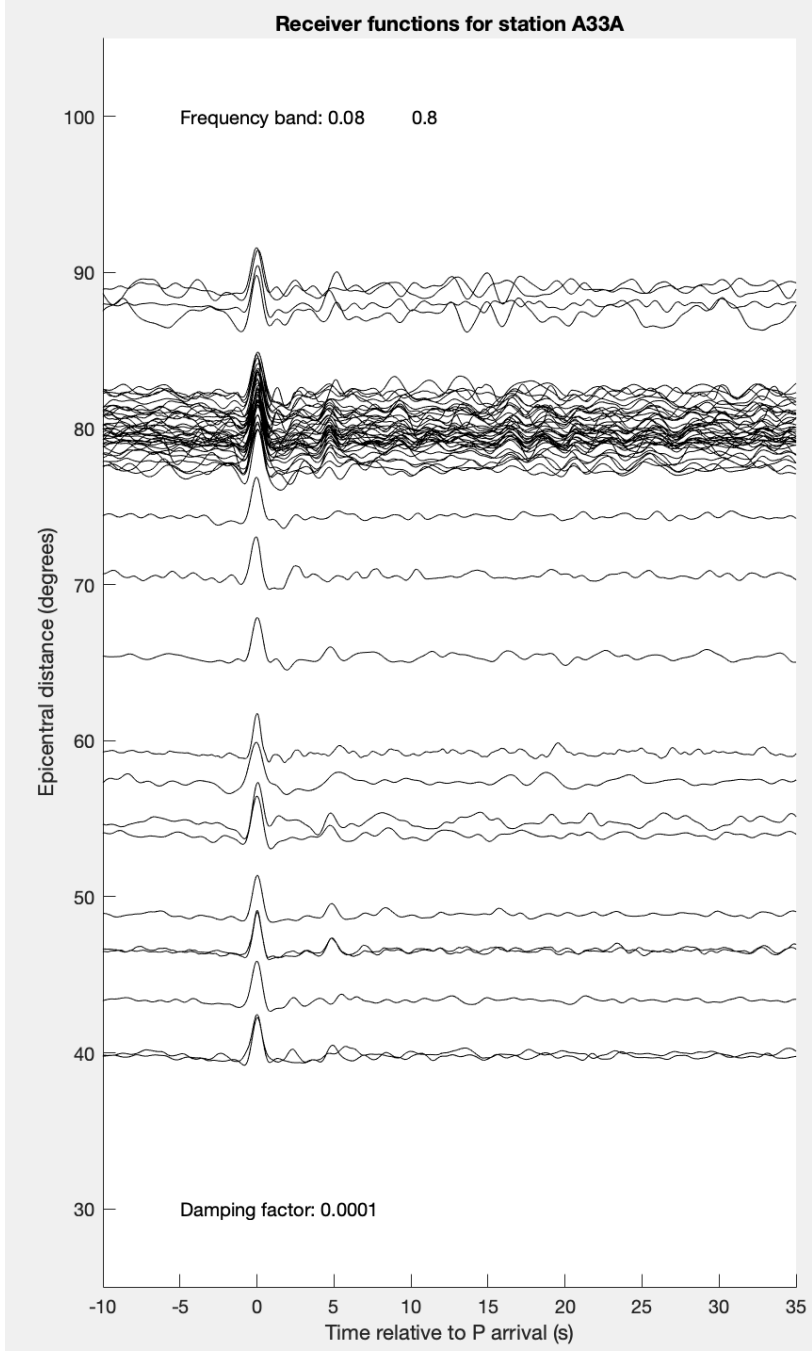


- A reminder: for simple crust, very little of the P coda appears on the vertical component of the impulse response – it's dominated by a single spike.
- This means that we can use the vertical component as an estimate of the source!
- So, receiver functions are typically produced by deconvolving the vertical component from the radial (and transverse).

- An example of raw teleseismic data from a site in Minnesota.
- Note how the waveforms are all different, and no converted arrivals are visible.



- After deconvolution, the waveforms are similar between events and we can see a clear Moho conversion at about 5 seconds.
- The dashed lines indicate the Moho Ps and two Moho multiples.



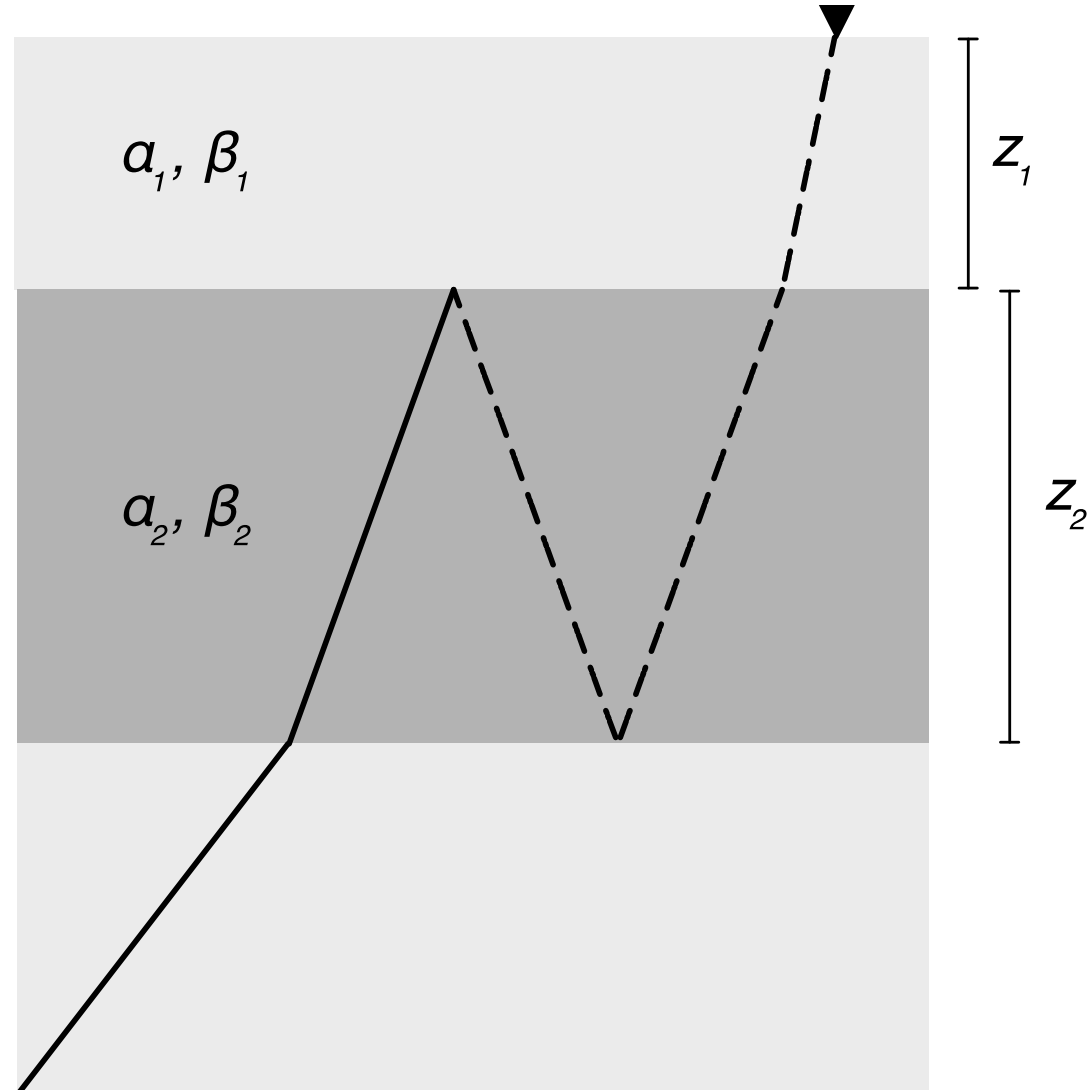
- There's a convenient expression for the travel time of a teleseismic pulse travelling through a stack of layers:

$$t = \sum_{j=1}^N z_j \xi_j$$

- This is a sum over all of the segments of the ray –  $z_j$  is the thickness of the layer traversed by segment  $j$ , and  $\xi_j$  is the vertical slowness in that ray:

$$\xi_j = \sqrt{1/c_j^2 - p^2}$$

- where  $c_j$  is the relevant layer velocity (P or S) and  $p$  is the ray parameter.



$$t = z_2 \sqrt{\frac{1}{\alpha_2^2} - p^2} + 2z_2 \sqrt{\frac{1}{\beta_2^2} - p^2} + z_1 \sqrt{\frac{1}{\beta_1^2} - p^2}$$

- For a single layer (e.g. the crust) of thickness  $H$ , the arrival time of the Ps conversion relative to P is:

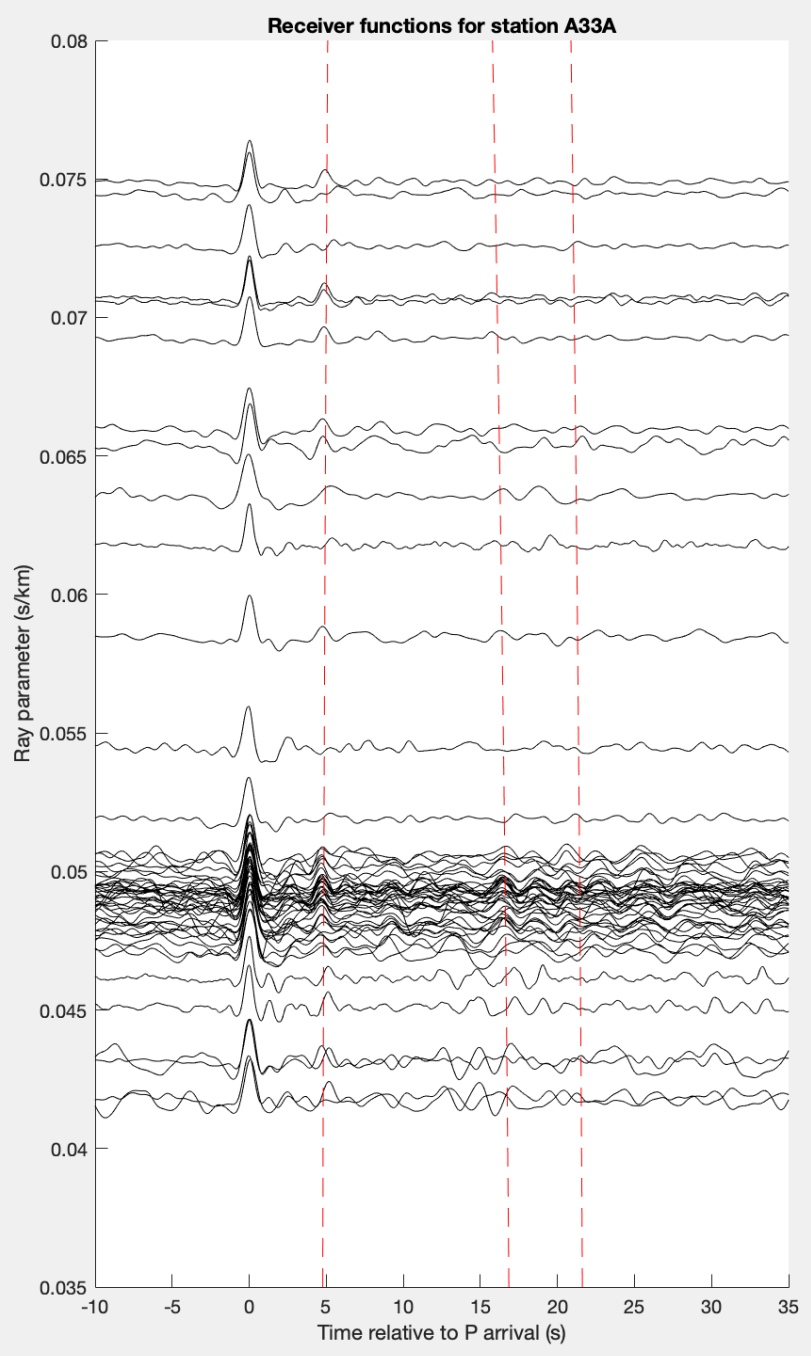
$$\delta t_{Ps} = H \left( \sqrt{1/\beta^2 - p^2} - \sqrt{1/\alpha^2 - p^2} \right)$$

- and the main multiples are

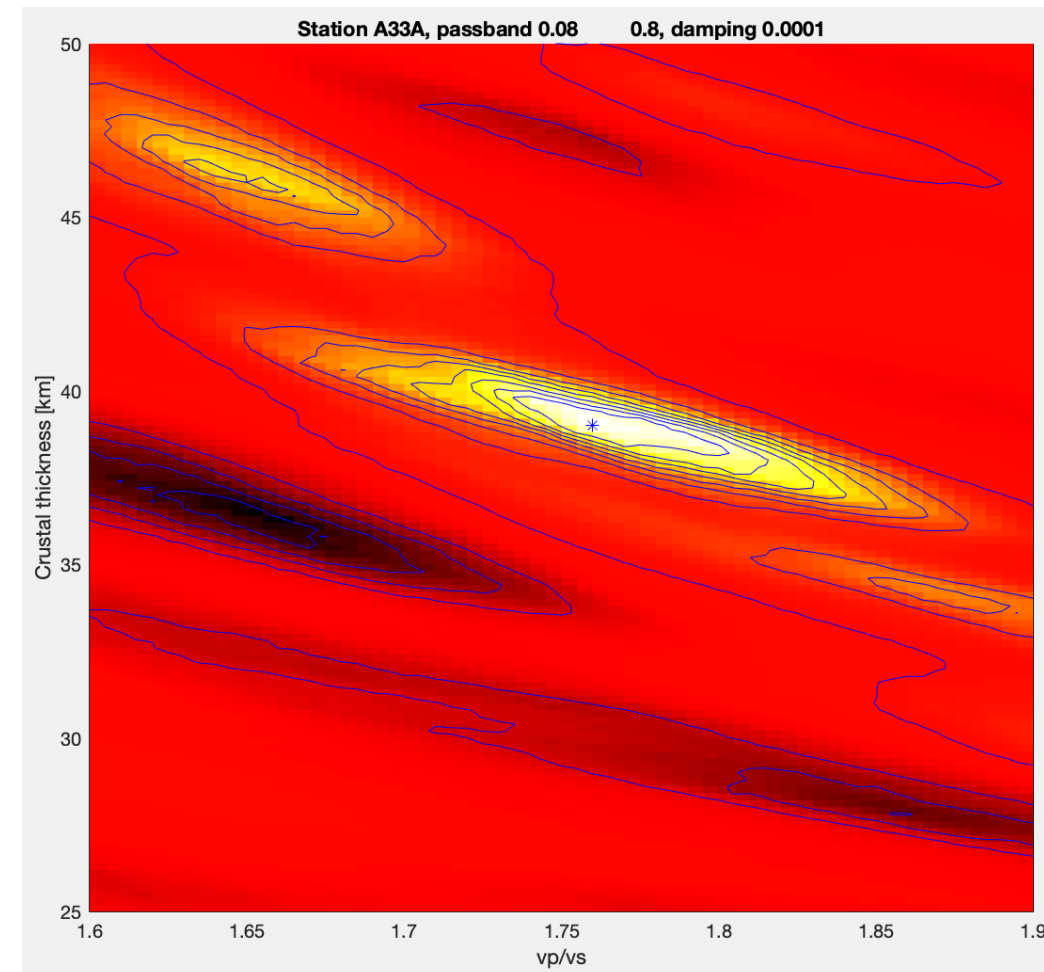
$$\delta t_{PpPs} = H \left( \sqrt{1/\beta^2 - p^2} + \sqrt{1/\alpha^2 - p^2} \right)$$

$$\delta t_{PpSS} = 2H \sqrt{1/\beta^2 - p^2}$$

- Note how these depend on both P and S velocity, and there's a velocity/depth tradeoff that is hard to resolve with the weak *moveout* (traveltime dependence on  $p$ ).
- However, these arrivals, **in combination**, may be used to constrain the ratio  $k = \alpha/\beta$ .



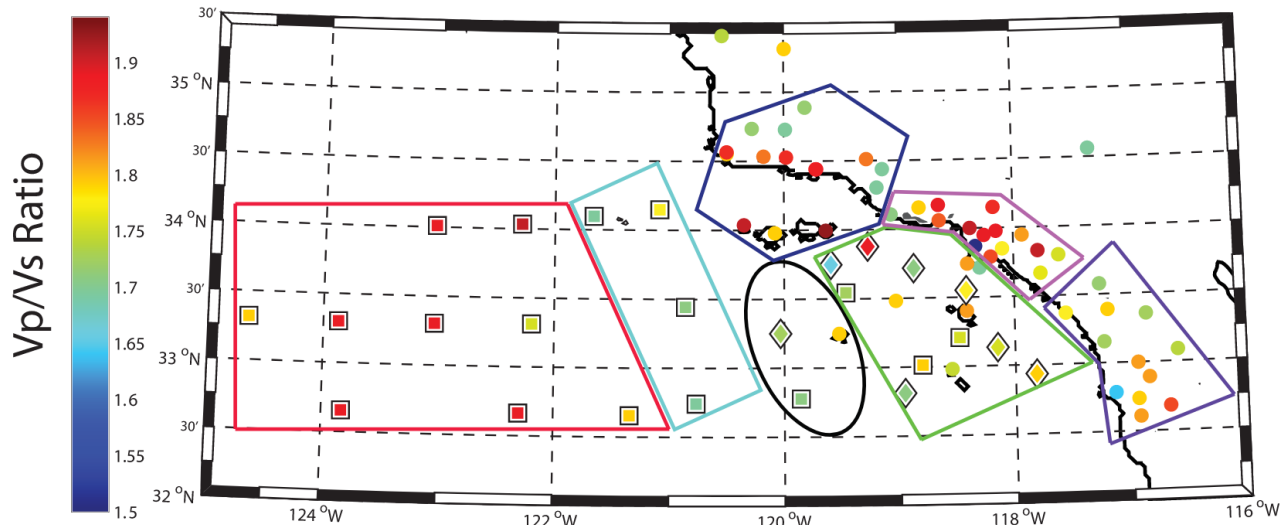
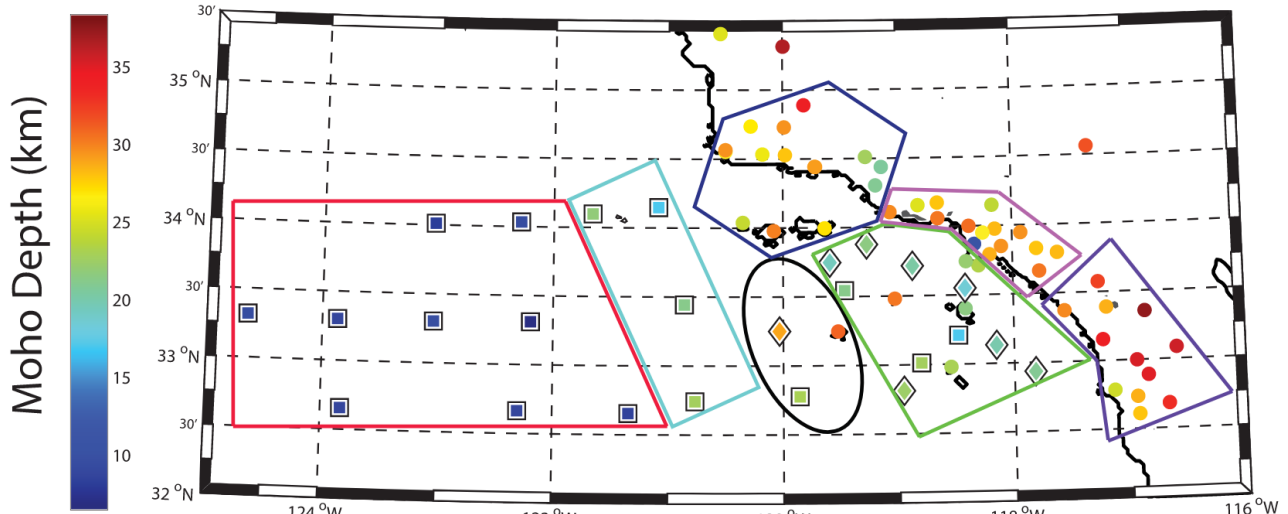
- The *H-k stacking technique* is a way of determining crustal thickness and P-S velocity ratio by stacking receiver functions on predicted arrival-time curves. The example below is an *H-k* stack of the traces at left – it works well at this station, which has clean Moho arrivals.



# OBS receiver functions

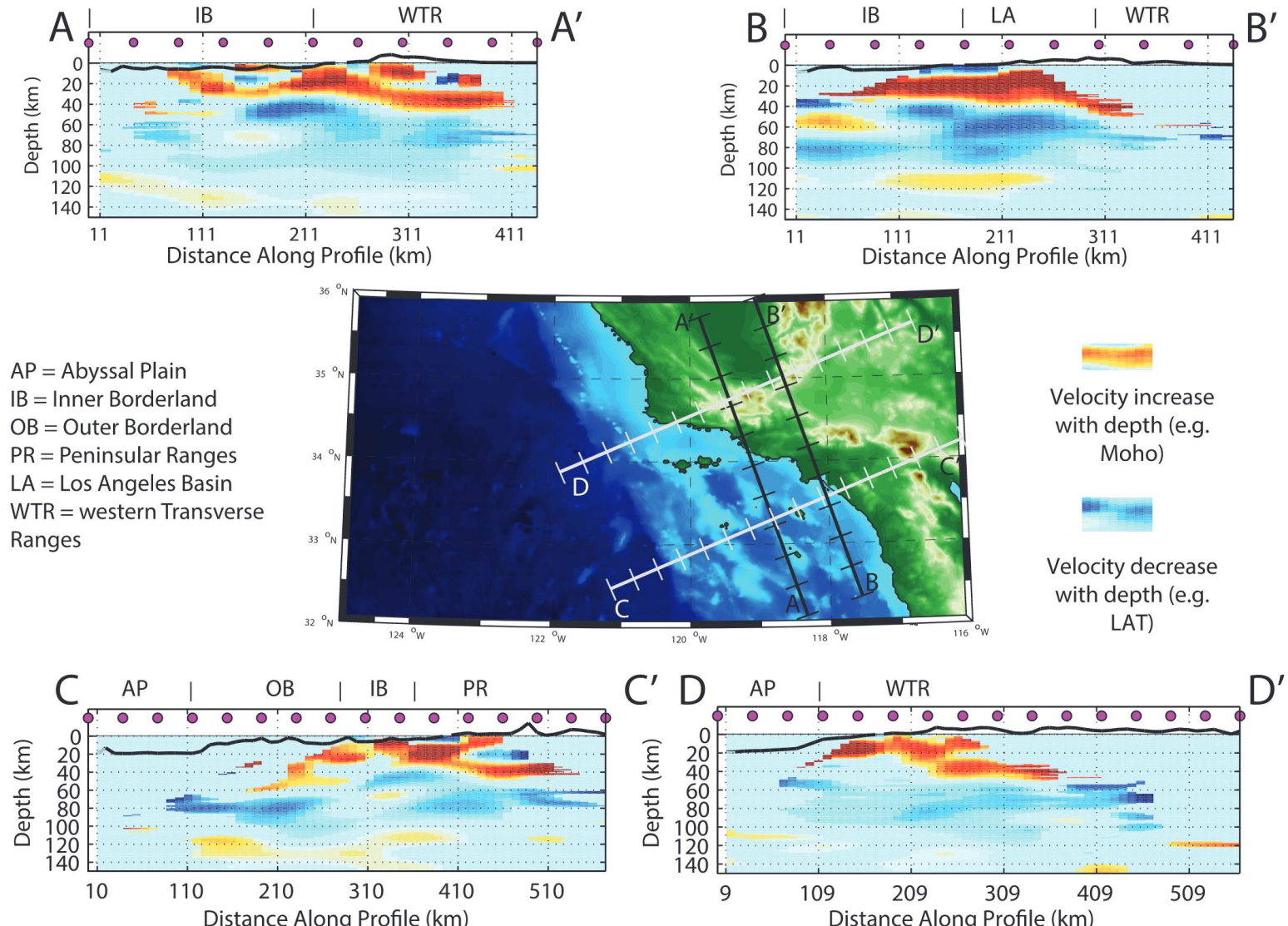
- Here's an  $H-k$  stacking example from an onshore-offshore study.
- Note the thinning of the crust heading seaward into the abyssal plain.
- The P/S velocity ratio tracks changes in the crustal composition, though note that this is an average that can include (e.g. in the far offshore region) significant unconsolidated sediment.

Reeves et al. (2014)

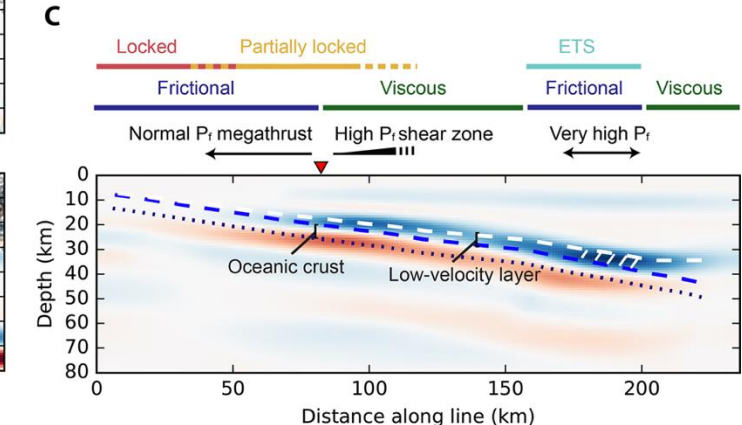
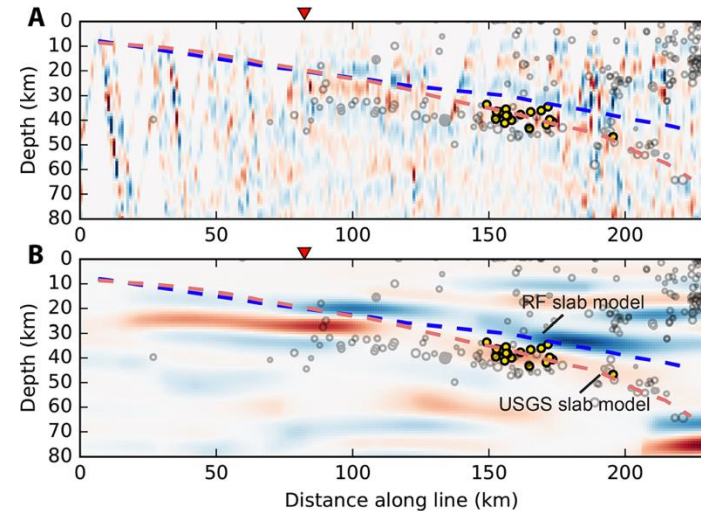
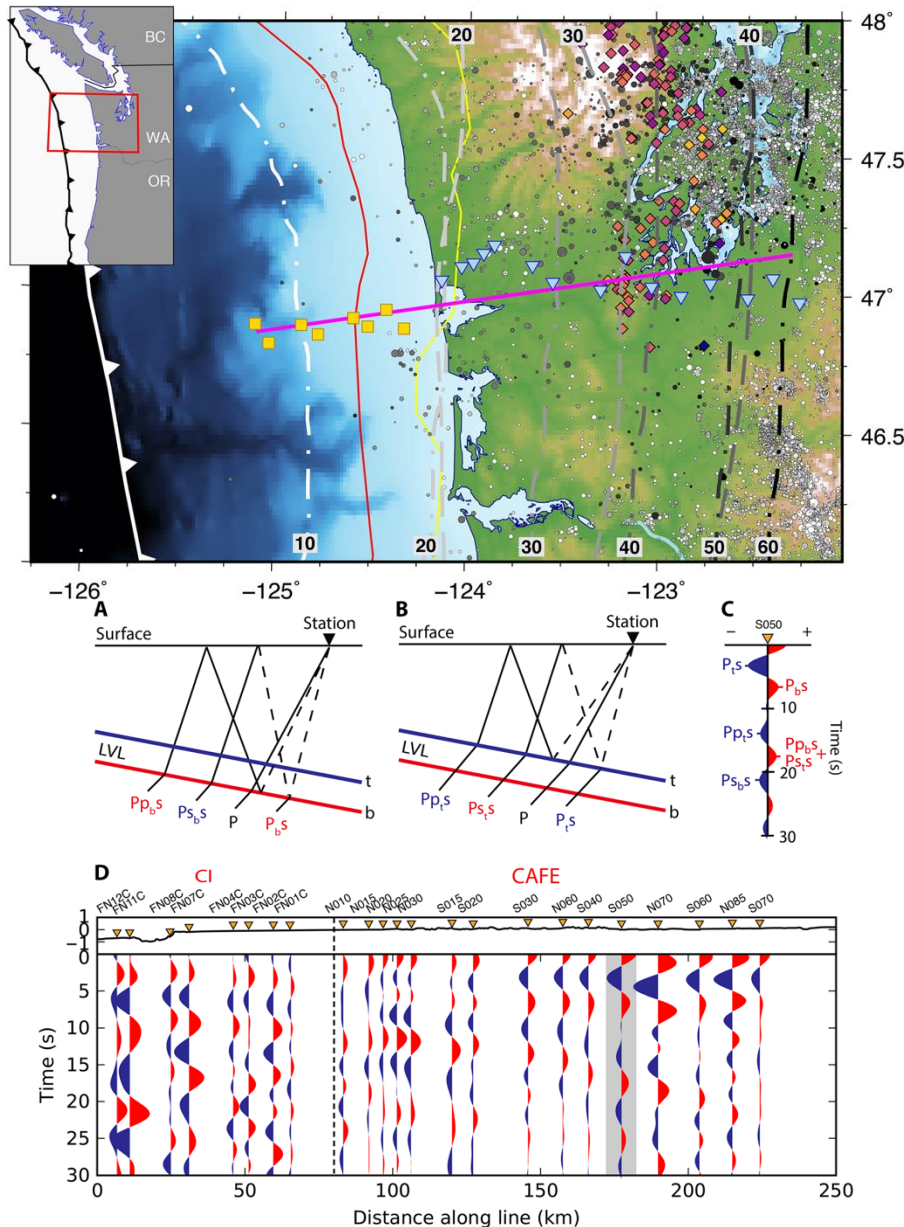


# OBS receiver functions

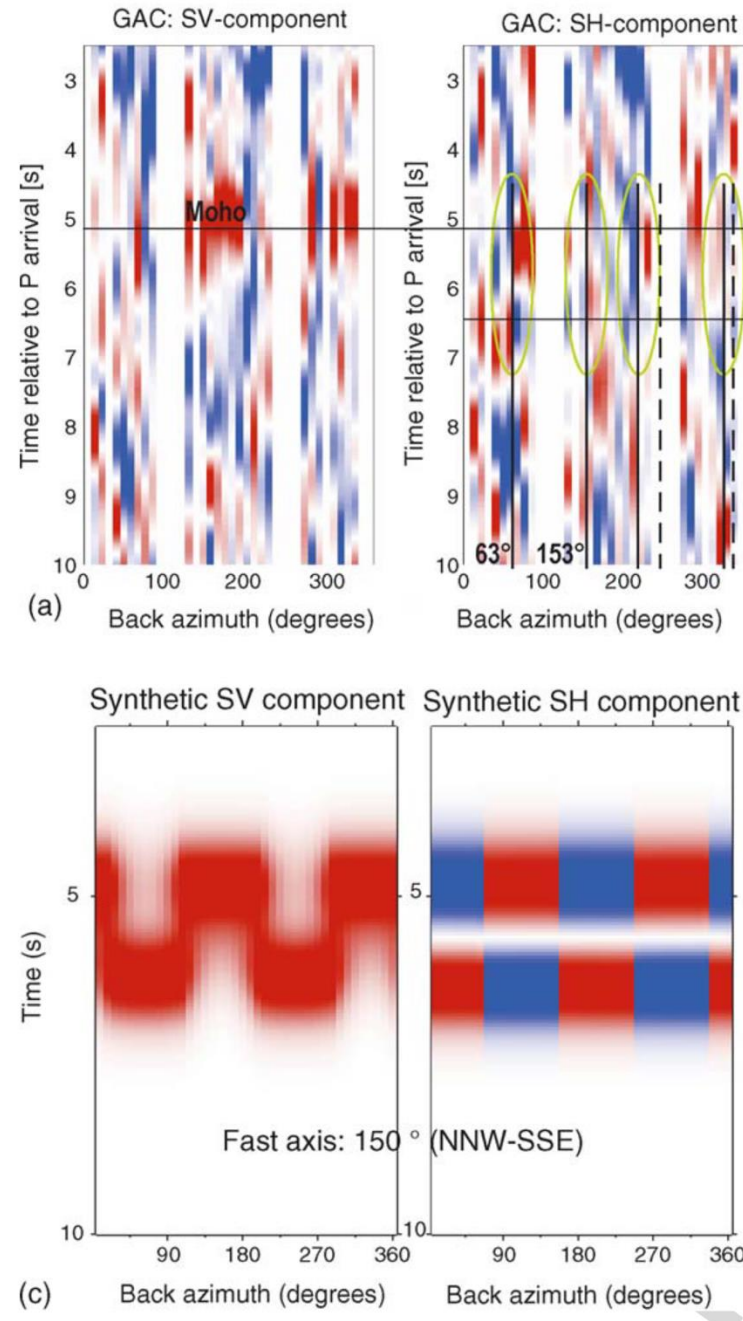
- The same study also includes another approach: common-conversion-point (CCP) stacking.
- In CCP stacking, every arrival is treated as a Ps conversion from a flat interface and assigned to its presumed conversion point in a 2-D section or 3-D volume. This requires assuming a velocity structure in advance – it's an *imaging* approach.
- Here you can see crust thickening landward, and the appearance of mid-crustal structure in the continental crust.



# OBS receiver functions



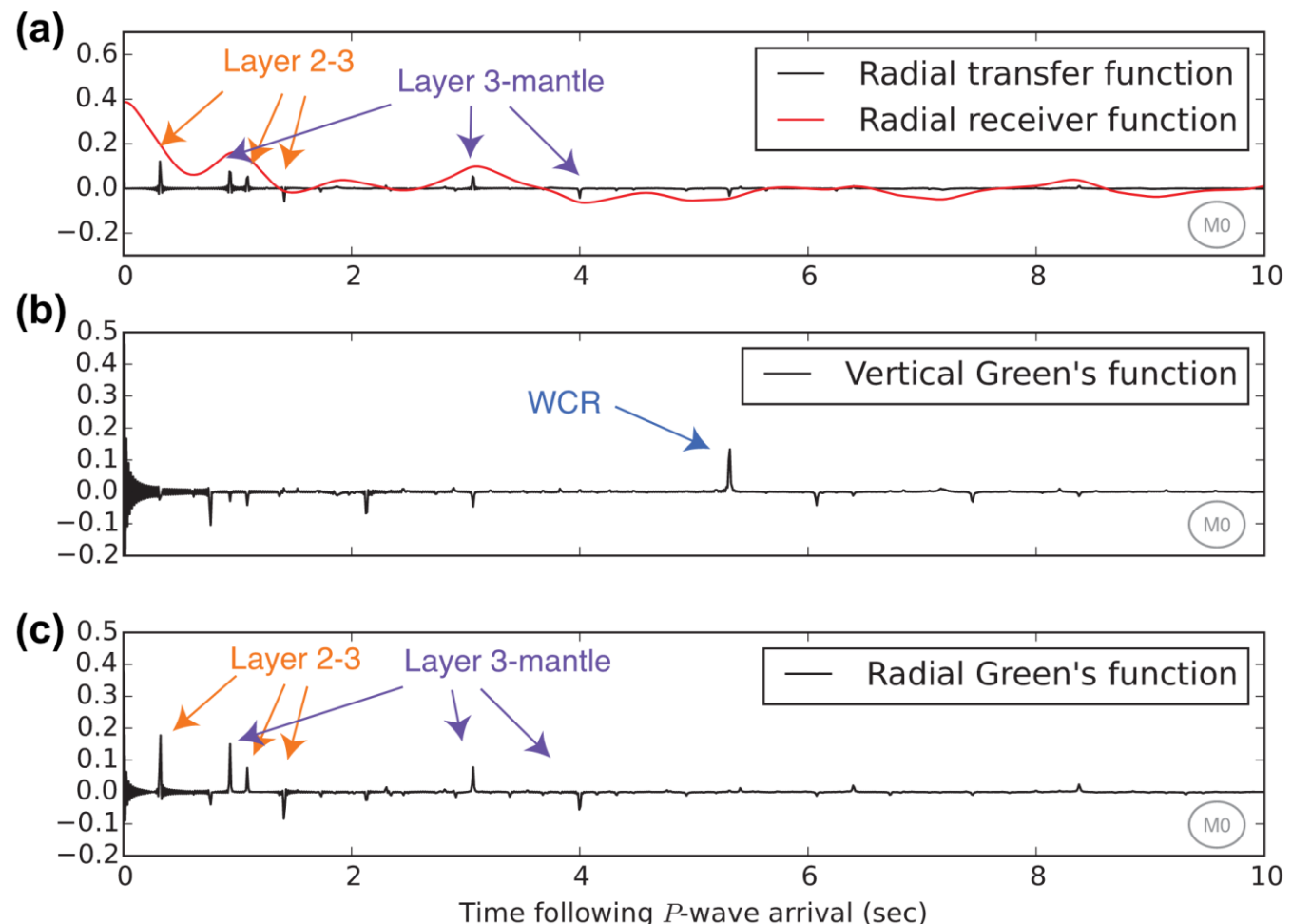
- CCP stacking can be done by combining all three phases (Ps, Pps & Pss)
- Example here from the Cascadia Initiative, with land + OBS stations, to resolve the shallow subduction zone structure.



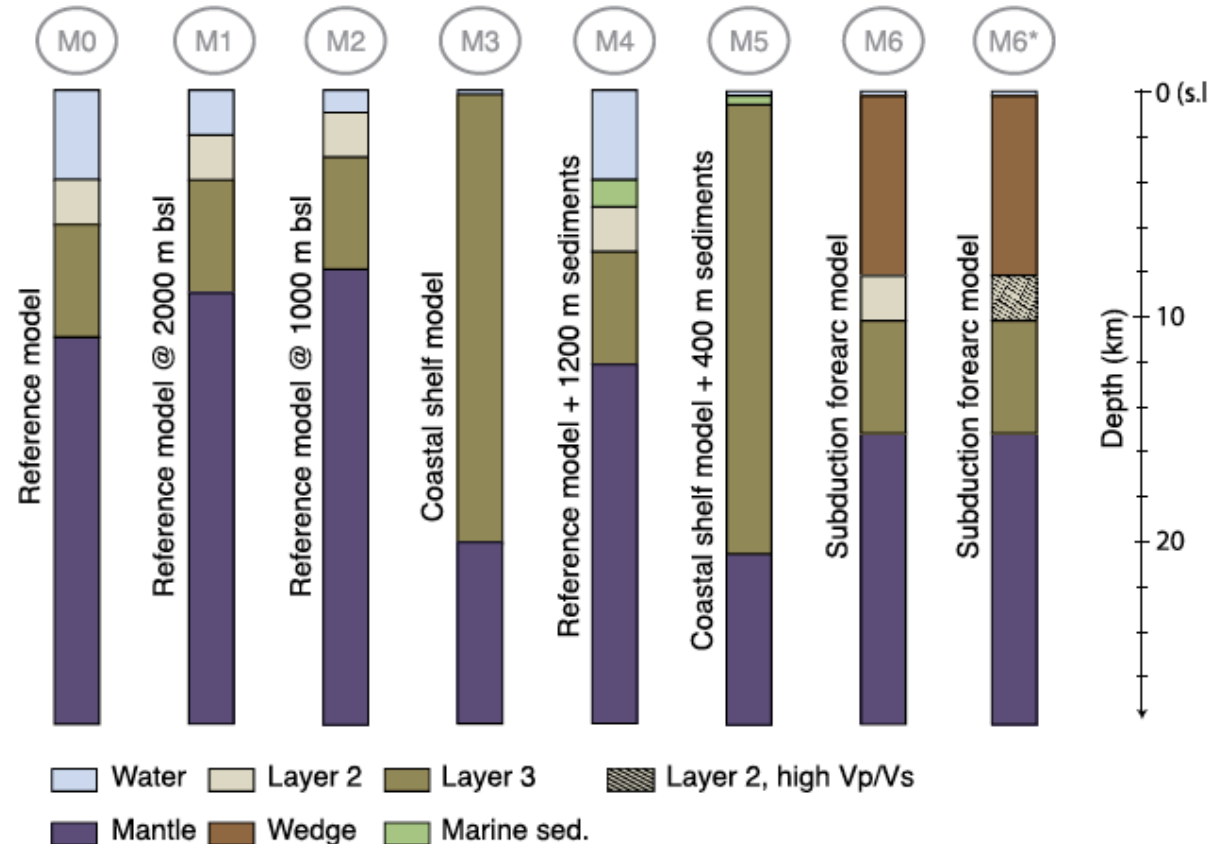
- With good back-azimuthal RF coverage and usable transverse components, it's possible to recover anisotropy or dip at a single station.
- This makes strong demands on the data, though, and will be challenging to do for OBS data given the combination of higher noise and short deployments.
- A good approach for this is *harmonic decomposition* to isolate anisotropic effects (see papers by I. Bianchi for examples).

# OBS receiver functions

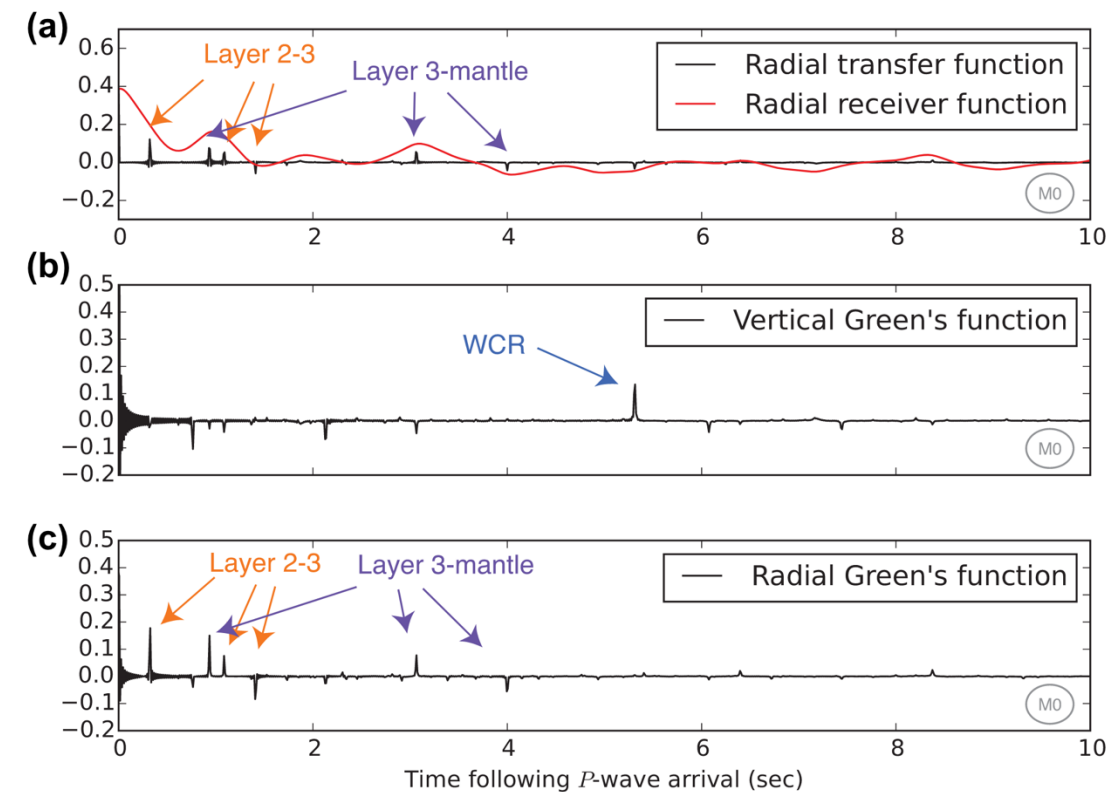
- Receiver functions can be challenging to work with in an offshore environment.
- In addition to higher noise levels and shorter deployments than on land, the marine environment itself can cause issues such as:
  - 1. Reverberations in the water column (“singing”)
  - 2. Reverberations in (often poorly consolidated) sediments.
  - These can obscure the Ps conversions we’re trying to observe.



# OBS receiver functions



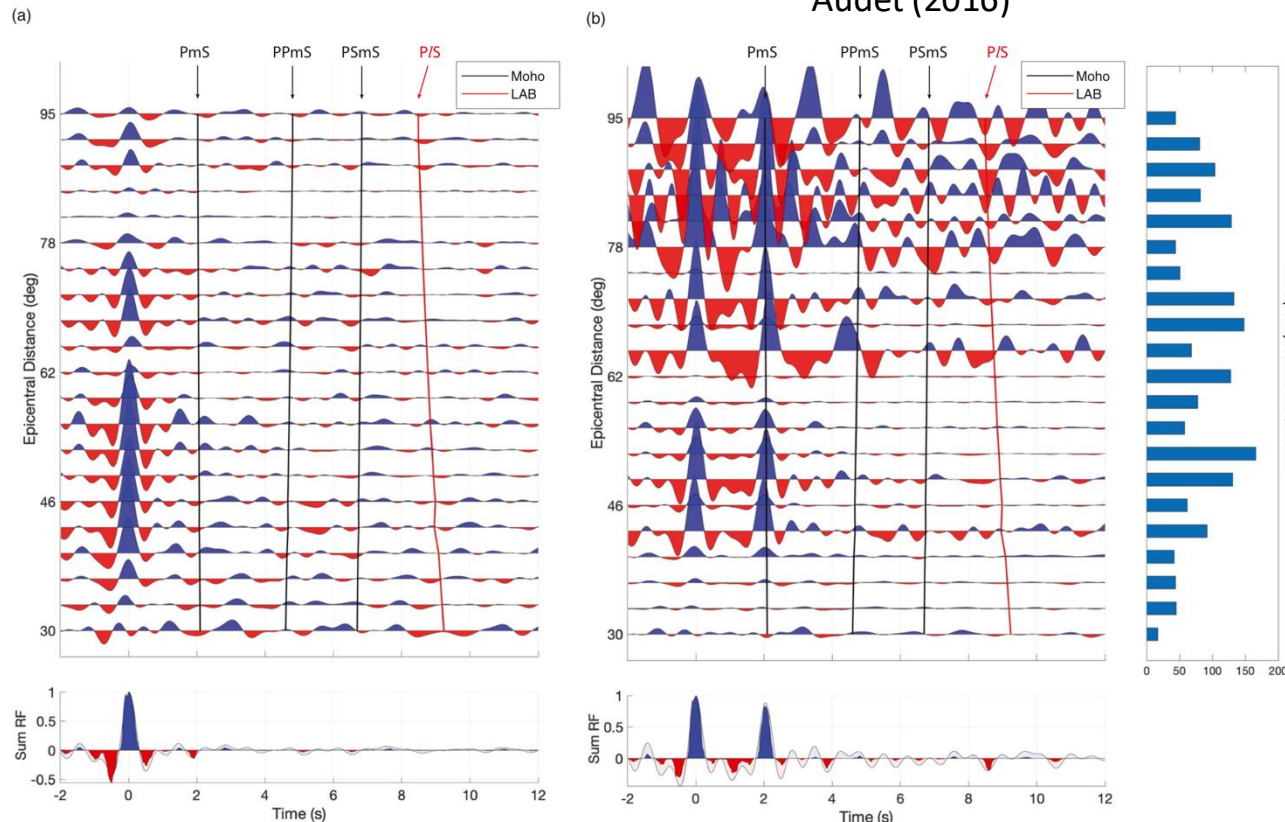
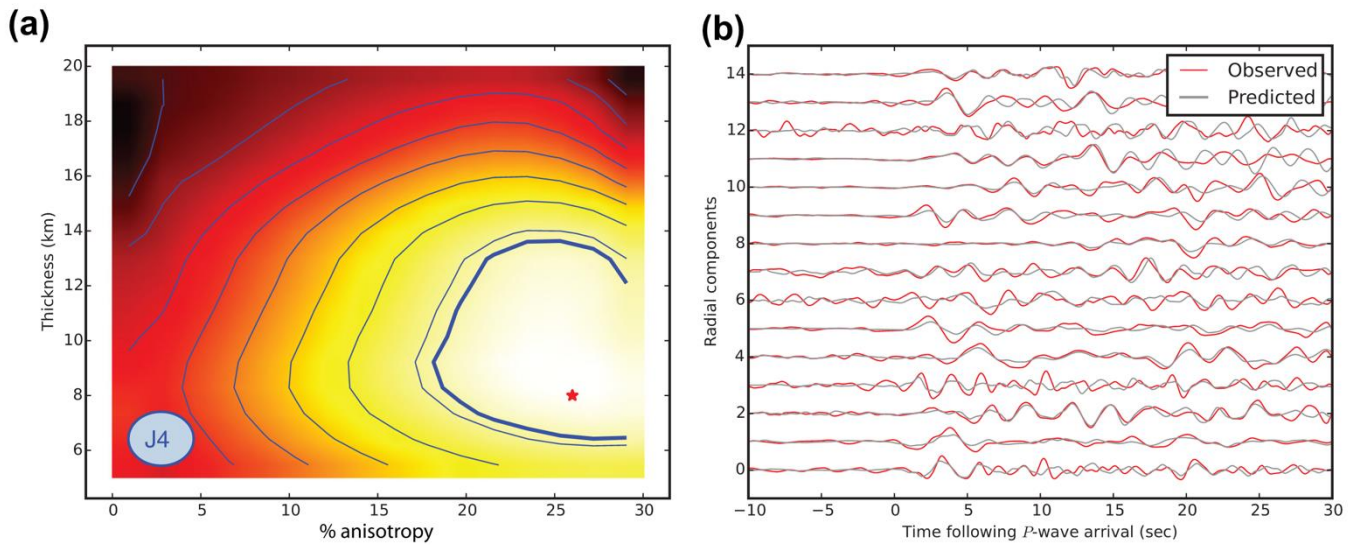
0 (s.l.)  
10  
20  
Depth (km)



- Check out examples in Audet (2016) for RFs in various structural environments.
- We will be able to reproduce those cases in Tutorial 5!

# Receiver functions

- The reverberations need to be either modelled (above) or removed (below).
- Practices for OBS receiver functions have not yet become standardized.
- You could invent something new here!



Zhang and Olugboji (2021)

# References

- Audet, P. (2016). Receiver functions using OBS data: Promises and limitations from numerical modelling and examples from the Cascadia Initiative. *Geophysical Journal International*, 205(3), 1740-1755. <https://doi.org/10.1093/gji/ggw111>
- Audet, P., & Schaeffer, A. J. (2018). Fluid pressure and shear zone development over the locked to slow slip region in Cascadia. *Science Advances*. <https://doi.org/aar2982>
- Darbyshire, F. A., Larsen, T. B., Voss, P. H., & Joyal, G. (2018). Crust and uppermost-mantle structure of Greenland and the Northwest Atlantic from Rayleigh wave group velocity tomography. *Geophysical Journal International*, 212(3), 1546-1569. <https://doi.org/10.1093/gji/ggx479>
- Eilon, Z. C., Zhang, L., Gaherty, J. B., Forsyth, D. W., & Russell, J. B. (2022). Sub-Lithospheric Small-Scale Convection Tomographically Imaged Beneath the Pacific Plate. *Geophysical Research Letters*, 49(18), e2022GL100351. <https://doi.org/10.1029/2022GL100351>
- Frederiksen, A., Ferguson, I., Eaton, D., Miong, S., & Gowan, E. (2006). Mantle fabric at multiple scales across an Archean–Proterozoic boundary, Grenville Front, Canada. *Physics of the Earth and Planetary Interiors*, 158(2-4), 240-263. <https://doi.org/10.1016/j.pepi.2006.03.025>
- Hammond, W. C., & Toomey, D. R. (2003). Seismic velocity anisotropy and heterogeneity beneath the Mantle Electromagnetic and Tomography Experiment (MELT) region of the East Pacific Rise from analysis of P and S body waves. *Journal of Geophysical Research: Solid Earth*, 108(B4). <https://doi.org/10.1029/2002JB001789>
- Harmon, N., Rychert, C. A., Kendall, J. M., Agius, M., Bogiatzis, P., & Tharimena, S. (2020). Evolution of the Oceanic Lithosphere in the Equatorial Atlantic From Rayleigh Wave Tomography, Evidence for Small-Scale Convection From the PI-LAB Experiment. *Geochemistry, Geophysics, Geosystems*, 21(9), e2020GC009174. <https://doi.org/10.1029/2020GC009174>

- Mojaver, O. B., Darbyshire, F., & Dave, R. (2021). Lithospheric Structure and Flat-Slab Subduction in the Northern Appalachians: Evidence From Rayleigh Wave Tomography. *Journal of Geophysical Research: Solid Earth*, 126(4), e2020JB020924. <https://doi.org/10.1029/2020JB020924>
- Petrescu, L., Darbyshire, F., Bastow, I., Totten, E., & Gilligan, A. (2017). Seismic anisotropy of Precambrian lithosphere: Insights from Rayleigh wave tomography of the eastern Superior Craton. *Journal of Geophysical Research: Solid Earth*, 122(5), 3754-3775. <https://doi.org/10.1002/2016JB013599>
- Reeves, Z., Lekić, V., Schmerr, N., Kohler, M., & Weeraratne, D. (2014). Lithospheric structure across the California Continental Borderland from receiver functions. *Geochemistry, Geophysics, Geosystems*, 16(1), 246-266. <https://doi.org/10.1002/2014GC005617>
- Saikia, U., Rychert, C., Harmon, N., & Kendall, J. M. (2021). Upper Mantle Anisotropic Shear Velocity Structure at the Equatorial Mid-Atlantic Ridge Constrained by Rayleigh Wave Group Velocity Analysis From the PI-LAB Experiment. *Geochemistry, Geophysics, Geosystems*, 22(3), e2020GC009495. <https://doi.org/10.1029/2020GC009495>
- Shapiro, N. M., & Campillo, M. (2004). Emergence of broadband Rayleigh waves from correlations of the ambient seismic noise. *Geophysical Research Letters*, 31(7). <https://doi.org/10.1029/2004GL019491>
- Tkalcic, H. (2017). *The Earth's Inner Core: Revealed by Observational Seismology*. Cambridge University Press.
- Zhang, Z., & Olugboji, T. (2021). The Signature and Elimination of Sediment Reverberations on Submarine Receiver Functions. *Journal of Geophysical Research: Solid Earth*, 126(5), e2020JB021567. <https://doi.org/10.1029/2020JB021567>